ARTICLE

doi:10.1038/nature24463

Genetic variation in glia–neuron signalling modulates ageing rate

Jiang-An Yin[1]*, Ge Gao[1,2]*, Xi-Juan Liu[1], Zi-Qian Hao[2,3], Kai Li[1], Xin-Lei Kang[1], Hong Li[4], Yuan-Hong Shan[5], Wen-Li Hu[5], Hai-Peng Li[3] & Shi-Qing Cai[1]

The rate of behavioural decline in the ageing population is remarkably variable among individuals. Despite the considerable interest in studying natural variation in ageing rate to identify factors that control healthy ageing, no such factor has yet been found. Here we report a genetic basis for variation in ageing rates in *Caenorhabditis elegans*. We find that *C. elegans* isolates show diverse lifespan and age-related declines in virility, pharyngeal pumping, and locomotion. DNA polymorphisms in a novel peptide-coding gene, named *regulatory-gene-for-behavioural-ageing-1* (*rgba-1*), and the neuropeptide receptor gene *npr-28* influence the rate of age-related decline of worm mating behaviour; these two genes might have been subjected to recent selective sweeps. Glia-derived RGBA-1 activates NPR-28 signalling, which acts in serotonergic and dopaminergic neurons to accelerate behavioural deterioration. This signalling involves the SIR-2.1-dependent activation of the mitochondrial unfolded protein response, a pathway that modulates ageing. Thus, natural variation in neuropeptide-mediated glia–neuron signalling modulates the rate of ageing in *C. elegans*.

Ageing is a major risk factor for many diseases, including neurodegenerative disorders, cancer, and diabetes[1]. With the rapid increase in the ageing population, the prevention of age-related functional impairment has emerged as an important medical challenge. Although most people experience the gradual and moderate declines of many functions as they age, some individuals undergo rapid or more extreme age-related declines whereas others maintain these functions throughout their lives, with only limited declines. It is thought that this discrepancy is at least in part attributable to genetic factors, particularly in view of the genome diversity among individuals[2]. Studies of the genetic origins of variability in the rate of ageing in animal models may provide new insights into the biological regulation of healthy ageing (that is, ageing that does not involve considerable decline in physiological functions).

Over the past three decades, our knowledge regarding the regulation of longevity has expanded greatly[1,3,4]. However, relatively little attention has been paid to the biological regulation of healthy ageing. Although longevity genes delay some cellular biomarkers of ageing[5–7], the extension of lifespan and the prevention of behavioural deterioration could be dissociable processes[8–13]. Recent whole-genome sequencing studies have revealed that genetic variants in people who age healthily are not correlated with those variants associated with exceptional longevity[11]. Thus, healthy ageing and longevity may to some extent be differentially regulated.

DNA polymorphisms can provide genetic diversity that is potentially advantageous for populations living in a range of environments; heritable variation is the raw material that shapes evolutionary change[14]. However, behavioural variation among populations within a given species generally has complex genetic foundations[15], and it remains a challenge to identify clear links between behavioural variation and specific DNA polymorphisms. As a result of its short lifespan and simple nervous system, the availability of powerful genetic tools, and the many wild strains isolated from different parts of the world, *C. elegans* is an excellent animal model not only for ageing research[3,4] but also for studying the genetic basis of behavioural variation[16–19]. In this study, we analyse the genetic basis of natural variation in ageing rates among wild strains of *C. elegans* and identify a novel glia-derived neuropeptide signalling pathway that modulates the rate of ageing.

Results

We analysed the rate of behavioural changes among wild strains of *C. elegans* during ageing and found that these wild strains showed diverse rates of age-related deterioration in virility, pharyngeal pumping, and locomotion (Fig. 1a–c). The N2 and JU258 strains showed rapid declines, whereas all other strains examined exhibited much slower declines in the mating efficiency of ageing males (Fig. 1a). This variation was not the result of differences in the behaviour of wild strains in leaving the colony[16,20]; all males showed similar levels of retention within the colony during the assay (Supplementary Table 1). Age-dependent decline in the pharyngeal pumping rate was moderate in the AB1, AB3, and reference N2 strains, but accelerated in the CB4856, CB4857, and RC301 strains, and slowed in all other strains that were tested (Fig. 1b). All strains showed similar declines in locomotor activity with the exception of CB4854, which exhibited higher locomotive activity during ageing (Fig. 1c). Further studies showed that there is a marked variation in lifespan among wild strains (Fig. 1d), and that slower functional declines are not always associated with longer lifespans (Fig. 1a–d).

Polymorphisms in *rgba-1* regulate male virility

To address the genetic basis of natural variation in the rate of ageing, we focused our study on the deterioration of male virility; of the three behaviours we examined, male virility showed the most pronounced variability. Age-dependent decline in the expression of BAS-1, the enzyme responsible for the synthesis of serotonin and dopamine[21], is known to contribute to the decay of virility in N2 males during ageing[9]. We thus assumed that aged wild strains with preserved male

[1]Institute of Neuroscience and State Key Laboratory of Neuroscience, CAS Center for Excellence in Brain Science and Intelligence Technology, Chinese Academy of Sciences, Shanghai, 200031, China. [2]University of Chinese Academy of Sciences, Beijing, 100049, China. [3]CAS Key Laboratory of Computational Biology, CAS-MPG Partner Institute for Computational Biology, Shanghai Institutes for Biological Sciences, Chinese Academy of Sciences, Shanghai, 200031, China. [4]Core Facility of Molecular Biology, Institute of Biochemistry and Cell Biology, Chinese Academy of Sciences, Shanghai, 200031, China. [5]Core Facility Center of the Institute of Plant Physiology and Ecology, Chinese Academy of Sciences, Shanghai, 200032, China.
*These authors contributed equally to this work.

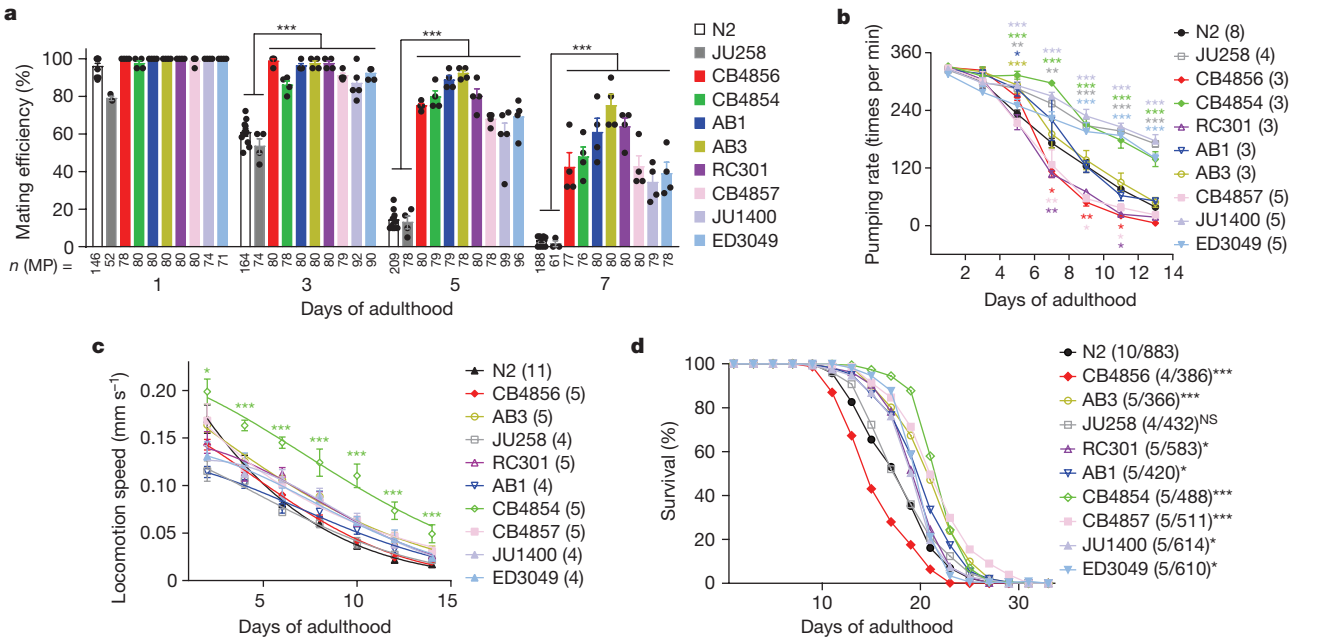

Figure 1 | Wild strains of *C. elegans* show varied ageing rates. a, Male mating efficiency for wild strains of *C. elegans*. Each data point represents the result of one independent experiment. MP, mating plates. **b**, **c**, Pharyngeal pumping rate (**b**) and locomotion speed (**c**) of wild strains. The numbers of independent assays are indicated in parentheses. **d**, Lifespan curves of wild strains. The numbers of assays and tested hermaphrodites are indicated in parentheses. For **a**–**c**, data shown are mean ± s.e.m. For **d**, data represent the sum of animals in multiple experiments. $*P < 0.05$, $**P < 0.01$, $***P < 0.001$, NS, not significant (**a**, two-way ANOVA; **b**, **c**, ANOVA with Dunnett's test; **d**, two-sided log-rank test). For **b**–**d**, the N2 strain was used as the reference for the comparison.

virility (for example, CB4856) may retain higher levels of BAS-1. About one-quarter of aged F2 (but not F1) progeny from a cross of N2 and CB4856 strains retained higher levels of BAS-1, suggesting that DNA polymorphisms in a specific gene regulate BAS-1 expression in aged worms. By backcrossing these F2 progeny with N2 worms eight times, we generated a new strain (SQC0002) that retained higher levels of BAS-1 and preserved male mating efficiency during ageing (Extended Data Fig. 1a–c).

Using whole-genome sequencing, we identified a 328-kb region of CB4856 genomic background in chromosome I of SQC0002 worms (Extended Data Fig. 1d). Further rescue experiments using fosmids and Mos1-mediated single-copy transgenes identified *F17B5.9*, which encodes a small protein with a signal peptide, putatively the precursor of a secreted neuropeptide (Fig. 2a and Extended Data Fig. 1e). We named this gene *rgba-1* (*regulatory-gene-for-behavioural-ageing-1*).

Using CRISPR–Cas9-mediated genome editing, we generated strains in which the 3G4H *rgba-1* allele in N2 worms was changed to 3V4H, 3G4R, or 3V4R (named *N2;rgba-1*^{3V4H}, *N2;rgba-1*^{3G4R}, and *N2;rgba-1*^{3V4R}, respectively, Extended Data Fig. 2a), to investigate whether polymorphisms of the signal peptide of RGBA-1 (Fig. 2b) affect male virility. Substituting the 3G4H *rgba-1* allele with the 3V4H, 3G4R, or 3V4R *rgba-1* allele enhanced mating efficiency in ageing N2 males (Fig. 2c). Furthermore, genome-edited CB4856 males (named *CB4856;rgba-1*^{3G4H}) in which the 3V4R *rgba-1* allele was replaced by the N2-type 3G4H allele (Extended Data Fig. 2a) displayed reduced mating efficiency at days 5 and 7 of adulthood (Fig. 2d). Thus, single nucleotide polymorphisms (SNPs) in *rgba-1* result in differing rates of decline in the virility of ageing males among wild strains.

RGBA-1 generates neuropeptides

We isolated total neuropeptides from N2 worms and separated them by high performance liquid chromatography (HPLC) (Extended Data Fig. 3a). Four peptides derived from RGBA-1 were identified by tandem mass spectrometry: RGBA-1-1a, RGBA-1-1b, RGBA-1-2a, and RGBA-1-2b (Fig. 2e and Extended Data Fig. 3b–f). Thus, *rgba-1* encodes endogenous neuropeptides.

The signal peptide of a neuropeptide precursor directs the protein into the endoplasmic reticulum for further proteolytic processing[22]. We found that the 3V4H, 3G4R, and 3V4R alleles impaired this function of the RGBA-1 signal peptide; mCherry-fused signal peptides with these alleles failed to co-localize with an endoplasmic reticulum marker protein (calnexin) in human embryonic kidney (HEK293T) cells, whereas RGBA-1 signal peptides with the 3G4H *rgba-1* allele showed normal function (Extended Data Fig. 4a, b). Furthermore, the presence of the 3V4H, 3G4R, or 3V4R allele reduced the accumulation of mRuby3-tagged RGBA-1 in coelomocytes (scavenger cells that endocytose macromolecules from the pseudocoelom of *C. elegans*[23]), suggesting that these alleles result in decreased RGBA-1 secretion (Extended Data Fig. 4c–f). Thus, 3V4H, 3G4R, and 3V4R are loss-of-function alleles. In support of this idea, CB4856 worms produced a lower amount of RGBA-1-2b than did N2 worms (Fig. 2e) and deletion of *rgba-1* in N2 worms prevented deterioration of mating ability in ageing males (Fig. 2f and Extended Data Fig. 2b). Thus, polymorphisms of *rgba-1* could regulate neuropeptide production, and loss-of-function *rgba-1* alleles prevent age-related declines in mating behaviours.

Expression of GFP under the control of the *rgba-1* promoter was found in the glial-like cells (including sheath, socket cells in both sexes, and ray structural cells of the male tail) and intestinal cells (Fig. 2g). To identify the site of action of RGBA-1, we deleted *rgba-1* in specific tissues by Cre–*LoxP*-mediated recombination (Extended Data Fig. 5a, b). Selective deletion of *rgba-1* in glial cells, but not neurons or intestinal cells, largely prevented the age-related decline in mating efficiency of N2 males (Fig. 2h and Extended Data Fig. 5c). Furthermore, re-expression of RGBA-1 in glial cells, but not neurons or intestinal cells, abolished the maintenance of mating efficiency in aged *rgba-1*-null males (Fig. 2i and Extended Data Fig. 5d–f). Thus, glia-derived neuropeptides regulate the rate of decline of male mating efficiency.

RGBA-1 activates NPR-28 signalling

We next sought to identify downstream effectors of RGBA-1. By RNA interference (RNAi) screening of 28 neuropeptide receptor genes, we found that downregulation of *npr-28*, which encodes a G-protein-coupled

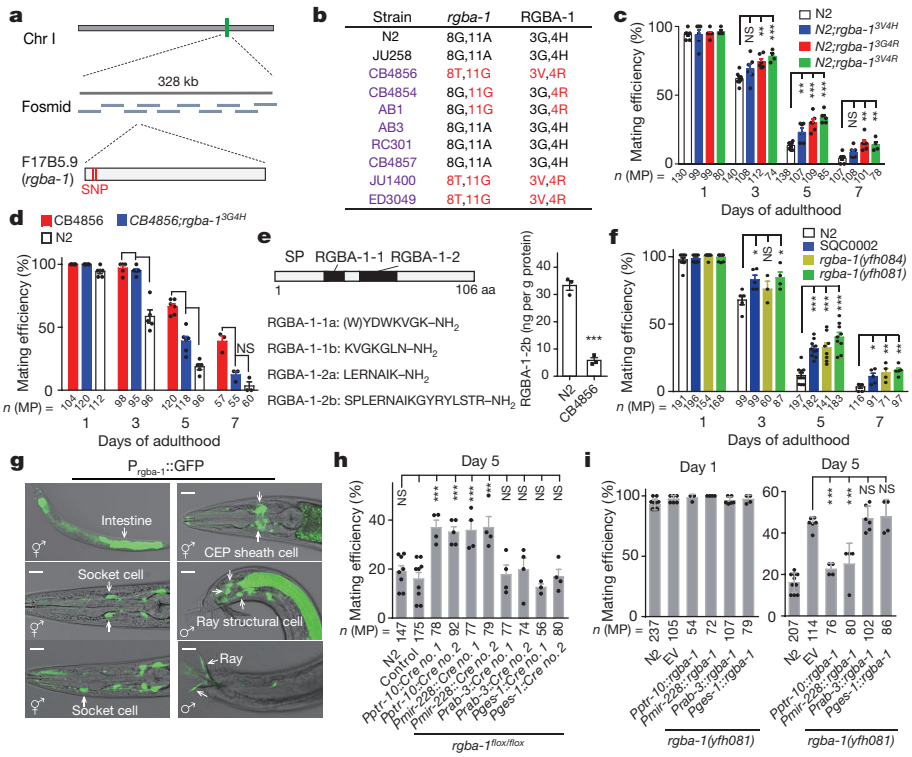

Figure 2 | Polymorphisms in *rgba-1* regulate mating efficiency. **a**, Cloning of *rgba-1*. The red lines indicate SNP sites. Chr I, chromosome I. **b**, Polymorphisms in *rgba-1*. **c**, Mating efficiency of N2, *N2;rgba-1*^{3V4H}, *N2;rgba-1*^{3G4R}, and *N2;rgba-1*^{3V4R} male worms. **d**, Mating efficiency of CB4856 and *CB4856;rgba-1*^{3G4H} male worms. **e**, Left, schematic of RGBA-1-derived neuropeptides. SP, signal peptide. Right, quantification of RGBA-1-2b in N2 and CB4856 worms. $n = 3$ assays. **f**, Mating efficiency of *rgba-1*-null male worms. **g**, RGBA-1 expression pattern in young adult worms. Scale bar, 15 μm. Representative of $n = 4$ independent experiments. **h**, Mating efficiency of N2 male worms at day 5 of adulthood with conditional deletion of *rgba-1* in glial cells (*rgba-1*$^{flox/flox}$;$P_{ptr\text{-}10}$::*Cre* or *rgba-1*$^{flox/flox}$;$P_{mir\text{-}228}$::*Cre*), neurons (*rgba-1*$^{flox/flox}$;$P_{rab\text{-}3}$::*Cre*), or intestinal cells (*rgba-1*$^{flox/flox}$;$P_{ges\text{-}1}$::*Cre*). Two independent transgenic lines per genotype were examined. **i**, Mating efficiency of *rgba-1* mutant male worms expressing a single copy of *rgba-1* in glial cells, neurons, or intestinal cells. EV, empty vector. All data shown are mean ± s.e.m. $^*P < 0.05$, $^{**}P < 0.01$, $^{***}P < 0.001$, NS, not significant (**c**, **d**, **f**, **h**, and **i**, ANOVA with Dunnett's test; **e**, two-sided *t* test). For **c**–**f**, **h**, and **i**, each data point represents the result of one independent experiment.

receptor with homology to somatostatin and nociceptin receptors, increased the level of BAS-1 (Extended Data Fig. 6a–c). Deletion of *npr-28* largely prevented the age-related decline in mating efficiency of N2 males (Fig. 3a and Extended Data Fig. 2c). The effects of *npr-28* and *rgba-1* on the mating efficiency of ageing males were not additive (Fig. 3a), suggesting that RGBA-1 and NPR-28 function in the same signalling pathway.

To further test this idea, we expressed *npr-28* cDNA in African green monkey fibroblast-like (COS-7) cells with the promiscuous G protein Gα16 (ref. 24), and administered synthetic peptides of RGBA-1 products. Cells expressing N2-type NPR-28 and Gα16 responded to RGBA-1-2b peptides at nanomolar concentrations, as indicated by Ca^{2+} elevation in the COS-7 cells (Fig. 3b, c); the other RGBA-1 peptides had no effect (Fig. 3b). Thus, RGBA-1 could activate cellular signalling mediated by NPR-28.

SNPs of *npr-28* modulate declines in male virility

An intron SNP, a synonymous SNP in exon 2, and a mis-sense SNP in exon 1 are present in *npr-28* (Table 1). The mis-sense SNP results in a substitution at the 166th residue, which was predicted to be located in the cytoplasmic side of the fourth transmembrane segment (Extended Data Fig. 6b). Compared with COS-7 cells transfected with the N2-type 166L *npr-28* allele, cells that expressed NPR-28 with the 166M allele showed markedly lower responses to RGBA-1-2b, with a more than tenfold increase in the half-maximal effective concentration (EC_{50}) for activating Ca^{2+} elevation (Fig. 3c), indicating that the 166M *npr-28* allele confers decreased receptor activity.

We then investigated whether *npr-28* SNPs affect the mating efficiency of ageing males. We generated two strains in the N2 genetic background: *N2;npr-28*^{166M} (with 166M replacing 166L) and *N2;npr-28*^{AB3} (in which the N2-type *npr-28* allele was replaced by the AB3-type *npr-28* allele) (Extended Data Fig. 2d), and found that aged *N2;npr-28*^{166M} and *N2;npr-28*^{AB3} males showed higher mating efficiencies than did age-matched N2 males (Fig. 3d). Furthermore, two genome-edited AB3 strains, in which the AB3-type *npr-28* was changed to 166L or the N2-type *npr-28* allele (*AB3;npr-28*^{166L} and *AB3;npr-28*^{N2}, respectively; Extended Data Fig. 2d), showed an accelerated decline in the mating efficiency of aged males (Fig. 3e). Thus, SNPs in *npr-28* produce variation in the rate of decline in mating efficiency of ageing males.

NPR-28 was broadly expressed in the head and tail neurons of both male and hermaphrodite worms (Fig. 3f). Further studies on the site of action of NPR-28 showed that when NPR-28 was specifically expressed in serotonergic or dopaminergic (but not GLR-1-expressing) neurons, it abolished the maintenance of virility in aged *npr-28*-null males (Fig. 3g and Extended Data Fig. 6d, e). Thus, NPR-28 acts in serotonergic and dopaminergic neurons to regulate mating efficiency.

The male mating behaviour of *C. elegans* includes multiple steps[25] (Extended Data Fig. 7a). The reduction in mating efficiency of aged N2 males is mainly attributable to progressive declines in turning, vulva locating, and sperm transfer abilities, but not to muscle weakness or sperm quality[26,27]. A substantial age-dependent reduction in the ability to perform three mating steps (turning, vulva locating, and sperm transfer), but not in the ability to perform the contact response to hermaphrodites, was observed in N2 males (Extended Data Fig. 7b–e), whereas these mating steps showed no (or minimal) decline in aged CB4856, AB3, *rgba-1*, and *npr-28* males (Extended Data Fig. 7b–e). Thus, RGBA-1–NPR-28 signalling could regulate multiple steps of male mating behaviour during ageing.

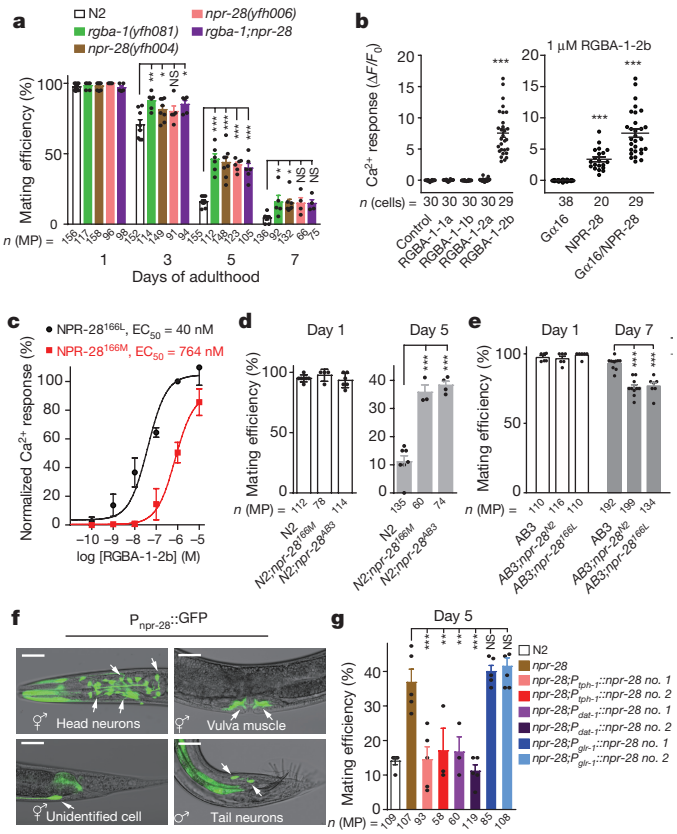

Figure 3 | Polymorphisms in *npr-28* regulate virility. a, Mating efficiency of *npr-28* and *rgba-1;npr-28* mutant male worms. **b**, Left, calcium responses of COS-7 cells expressing N2-type NPR-28 and Gα16, exposed to 1 μM synthetic RGBA-1-derived neuropeptides. Vehicle was used as the control. Right, calcium responses of COS-7 cells expressing N2-type NPR-28, exposed to 1 μM synthetic RGBA-1-2b. GCaMP6f was co-expressed in the cells to measure the calcium signal. **c**, Dose–response curves of COS-7 cells expressing NPR-28^{166L} (or NPR-28^{166M}) and Gα16. Data were fitted by nonlinear regression. **d**, **e**, Mating efficiency of N2, *N2;npr-28^{166M}*, and *N2;npr-28^{AB3}* male worms (**d**), and of AB3, *AB3;npr-28^{N2}*, and *AB3;npr-28^{166L}* male worms (**e**). **f**, NPR-28 expression in young adult worms. Scale bar, 25 μm. Representative of $n = 3$ independent experiments. **g**, Mating efficiency of *npr-28*-null males selectively expressing N2-type NPR-28 in serotonergic (driven by *tph-1* promoter), dopaminergic (driven by *dat-1* promoter), and motor (or inter-) neurons (driven by *glr-1* promoter) at day 5 of adulthood. Two independent transgenic lines per genotype were examined. All data shown are mean ± s.e.m. $*P < 0.05$, $**P < 0.01$, $***P < 0.001$, NS, not significant (ANOVA with Dunnett's test). For **a**, **d**, **e**, and **g**, each data point represents the result of one independent experiment. The numbers of mating plates (for **a**, **d**, **e**, and **g**) or cells (for **b**) are shown beneath the bars.

We next investigated whether RGBA-1–NPR-28 signalling affects the ageing rates of other behaviours. Null mutations in *rgba-1* and *npr-28* delayed the age-dependent deterioration in pharyngeal pumping (Extended Data Fig. 7f), but only marginally affected locomotor activity and lifespan (Extended Data Fig. 7g, h), of N2 worms. Thus, the signalling involved in regulating the behaviours in ageing animals could be dissociated from the signalling that influences longevity.

RGBA-1 and NPR-28 regulate UPR^{mt} via SIR-2.1

The conserved NAD$^+$-dependent protein deacetylase SIR-2.1 (refs 28, 29) has been implicated in the decline in male virility in early-ageing *C. elegans*[30]. We found that the null mutation of *sir-2.1* fully abolished the maintenance of virility in ageing *rgba-1* and *npr-28* mutant males (Fig. 4a), indicating that the effect of RGBA-1–NPR-28 signalling on the decline of virility depends on the presence of SIR-2.1. The decline in male virility in *sir-2.1*-null and aged N2 males has in part been attributed to altered metabolic homeostasis[30]. However, aged *rgba-1* and *npr-28* mutant males showed levels of expression of catabolic enzymes and ROS-scavengers comparable to those of age-matched N2 males (Extended Data Table 1), suggesting that RGBA-1–NPR-28 signalling regulates the virility of ageing males through other mechanisms.

Table 1 | Polymorphisms in *rgba-1* and *npr-28* genes

Strain	*rgba-1*	RGBA-1	*npr-28*	NPR-28	Mating efficiency
N2	8G, 11A	3G, 4H	496T, 1172C, 1220T	166L	Low
JU258	8G, 11A	3G, 4H	496T, 1172C, 1220T	166L	Low
CB4856	8T, 11G	3V, 4R	496T, 1172C, 1220T	166L	High
CB4854	8G, 11G	3G, 4R	496A, 1172T, 1220C	166M	High
AB1	8G, 11G	3G, 4R	496A, 1172T, 1220C	166M	High
AB3	8G, 11A	3G, 4H	496A, 1172T, 1220C	166M	High
RC301	8G, 11A	3G, 4H	496A, 1172T, 1220C	166M	High
CB4857	8G, 11A	3G, 4H	496T, 1172T, 1220C	166L	High
JU1400	8T, 11G	3V, 4R	496T, 1172T, 1220C	166L	High
ED3049	8T, 11G	3V, 4R	496A, 1172T, 1220C	166M	High

SIR-2.1 is a regulator for the mitochondrial unfolded protein response (UPR^{mt})[31,32], which is known to promote longevity[33,34]. The *rgba-1* and *npr-28* mutant worms showed enhanced transcription of the UPR^{mt}-related genes *hsp-6*, *hsp-60* and *clpp-1* (Extended Data Table 1), and the activation of UPR^{mt} (also indicated by the UPR^{mt} reporter in which GFP is driven by the *hsp-6* promoter (P_{hsp-6}::GFP)[35]) was considerably attenuated by the null mutation of *sir-2.1* (Fig. 4b and Extended Data Fig. 8a). Suppression of UPR^{mt} by RNAi directed against *ubl-5*, which encodes an ubiquitin-like protein that positively regulates UPR^{mt} (ref. 36), abolished the maintenance of virility in ageing *rgba-1* and *npr-28* mutant males (Fig. 4c and Extended Data Fig. 8a, b). Therefore, RGBA-1–NPR-28 signalling regulates the virility of aged males by modulating the activation of UPR^{mt}. The transcription level of *hsp-6*, *hsp-60*, and *clpp-1* in aged CB4856 and AB3 worms was higher than in age-matched N2 worms (Extended Data Table 1), and RNAi of *ubl-5* substantially reduced the virility of aged CB4856 and AB3 males (Fig. 4d), suggesting that the UPR^{mt} is critical in generating natural variation in the rate of ageing.

Population genetics of *rgba-1* and *npr-28*

No RGBA-1 homologues have been found in other nematode species, suggesting that *rgba-1* is a new gene in *C. elegans*. Population genetic analysis of DNA polymorphism data, from the *C. elegans* Natural Diversity Resource (www.elegansvariation.org), showed that the 20-kb genomic region centred on *rgba-1* might have been subjected to a recent selective sweep, with a Tajima's *D* value of −2.31 (one-tailed test, $P = 4.9 \times 10^{-5}$) and an unbalanced phylogenetic tree (unbalanced test[37], $P = 0.048$) (Extended Data Fig. 9a). We also found evidence for a selective sweep on the 20-kb genomic region encompassing *npr-28*, as suggested by a Tajima's *D* value of −1.47 (one-tailed test, $P = 0.033$) and an unbalanced test ($P = 0.04$) (Extended Data Fig. 9a). These results are in agreement with the findings of chromosome-scale selective sweeps[38].

All *rgba-1* and *npr-28* alleles are found globally (Extended Data Fig. 9b). To identify the ancestral or derived status of these alleles, we constructed dendrograms across 18 wild strains using the 20-kb genomic region centred on *rgba-1* or *npr-28*. According to the principle of parsimony[39], we inferred that the 3G and 4R alleles in *rgba-1* and the 166L allele in *npr-28* are ancestral, whereas the 3V and 4H alleles in *rgba-1* and the 166M allele in *npr-28* are derived (Fig. 5a, b and Extended Data Fig. 6f). All of the tested wild strains with the 4R allele in *rgba-1* or the 166M allele in *npr-28*, or both, showed a high mating efficiency in aged males (Fig. 5a-c), consistent with the finding that these two alleles prevent age-related declines in virility (Figs 2b–d, 3d, e). Eight of the tested wild strains carry the 3G4H allele in *rgba-1* and the 166L allele in *npr-28*. Five of them (including JU258, shown in Fig. 1a) underwent fast declines, whereas the other three strains exhibited slow age-related declines in mating ability (Fig. 5c). Because

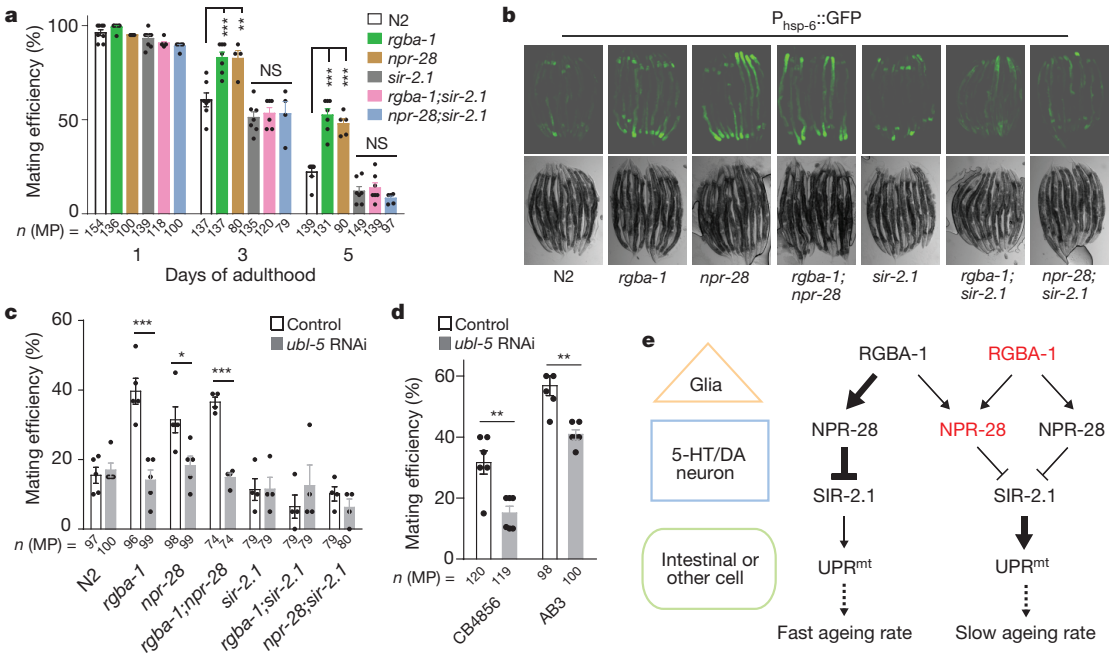

Figure 4 | RGBA-1–NPR-28 signalling regulates UPR^{mt} via SIR-2.1. **a**, The effect of SIR-2.1 on mating efficiency of ageing *rgba-1*- and *npr-28*-null male worms. **b**, Fluorescent images of worms expressing the UPR^{mt} reporter $P_{hsp\text{-}6}$::GFP. Representative of $n = 3$ independent experiments. **c**, Mating efficiency of males at day 5 of adulthood in the absence or presence of *ubl-5* RNAi. **d**, The effect of *ubl-5* RNAi on mating efficiency in CB4856 and AB3 males at day 7 of adulthood. **e**, Proposed model for regulation of ageing rate. N2-type and loss-of-function *rgba-1* (or *npr-28*) alleles are highlighted in black and red, respectively. All data shown are mean ± s.e.m. $*P < 0.05$, $**P < 0.01$, $***P < 0.001$, NS, not significant (**a**, ANOVA with Dunnett's test; **c**, **d**, two-sided *t* test). For **a**, **c**, and **d**, each data point represents the result of one independent experiment.

no polymorphism was found in *rgba-1* and *npr-28* among these eight strains, this result suggests the existence of further genes (besides *rgba-1* and *npr-28*) with polymorphisms that contribute to natural variation in ageing rates. Evolution in ageing rates may, therefore, have been affected by natural polymorphisms in *rgba-1* and *npr-28*, as well as other genes.

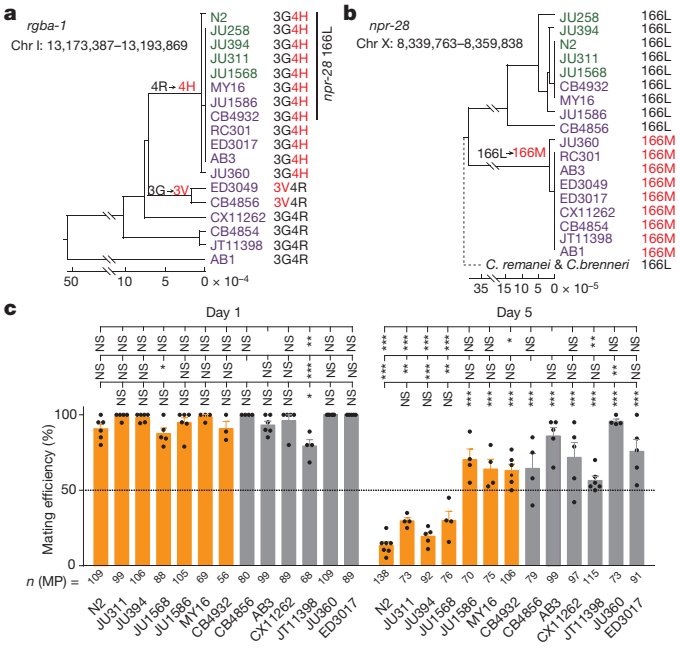

Figure 5 | Population genetics of *rgba-1* and *npr-28* loci. **a**, **b**, Dendrograms of 18 natural isolates using the 20-kb genomic region surrounding *rgba-1* (**a**) or *npr-28* (**b**). Ancestral and derived alleles are shown in black and red, respectively. **c**, Mating ability of wild strains. Wild strains that carry N2-type *rgba-1* and N2-type *npr-28* alleles are highlighted in orange. Each data point represents the result of one independent experiment. Data shown are mean ± s.e.m. $*P < 0.05$, $**P < 0.01$, $***P < 0.001$, NS, not significant (ANOVA with Dunnett's test).

Discussion

In this study of *C. elegans* wild strains, we found that lifespan and the behavioural declines associated with ageing are highly variable. We demonstrated that DNA polymorphisms in *rgba-1* and *npr-28* influence the rate of age-related decline of worm mating behaviour, and that these two genes might have been subjected to recent selective sweeps. Furthermore, glia-derived RGBA-1 neuropeptides activate NPR-28 receptor signalling in serotonergic and dopaminergic neurons, leading to a reduction in SIR-2.1-mediated activation of UPR^{mt}, which is known to modulate ageing (Fig. 4e). Our work, therefore, suggests a genetic mechanism underlying natural variation in the rate of ageing and provides insight into the biological regulation of healthy ageing.

The antagonistic pleiotropy theory of the evolution of ageing proposes that naturally selected pleiotropic genes offer benefits early in life, but produce detrimental effects as an organism ages[40]. This has led to the view that healthspan is evolutionarily optimized[12,40]. In support of this hypothesis, lifespan extension in long-lived mutant worms occurs at a measurable fitness cost[12,41–44]. However, the existence of individuals that display both a long lifespan and vigorous behaviours throughout this lifespan suggests that it is possible to extend both healthspan and lifespan. The evolutionary selection of genes that promote survival and reproductive success in early life could also result in a concomitant reduction in the rate of behavioural decline or extension of lifespan, or both.

Ageing variation among populations may have complex genetic bases. RGBA-1–NPR-28 signalling affects only some aspects of healthy ageing; it had little effect on the lifespan and age-dependent decline in locomotion. Mammalian neuropeptide Y has been demonstrated to modulate ageing[45,46]. Polymorphisms in the mammalian neuropeptide Y gene affect the production and secretion of this peptide[47]; neuropeptide

pathways may, therefore, be a general mechanism that underlies natural variation in the rate of ageing. Further study of long-lived *C. elegans* wild strains that preserve physiological functions into their late adulthood will extend our understanding of the biological regulation of healthy ageing.

Online Content Methods, along with any additional Extended Data display items and Source Data, are available in the online version of the paper; references unique to these sections appear only in the online paper.

Received 22 February; accepted 2 October 2017.

1. López-Otín, C., Blasco, M. A., Partridge, L., Serrano, M. & Kroemer, G. The hallmarks of aging. *Cell* **153,** 1194–1217 (2013).
2. Sachidanandam, R. *et al.* A map of human genome sequence variation containing 1.42 million single nucleotide polymorphisms. *Nature* **409,** 928–933 (2001).
3. Gems, D. & Partridge, L. Genetics of longevity in model organisms: debates and paradigm shifts. *Annu. Rev. Physiol.* **75,** 621–644 (2013).
4. Kenyon, C. J. The genetics of ageing. *Nature* **464,** 504–512 (2010).
5. Herndon, L. A. *et al.* Stochastic and genetic factors influence tissue-specific decline in ageing *C. elegans*. *Nature* **419,** 808–814 (2002).
6. Cohen, E., Bieschke, J., Perciavalle, R. M., Kelly, J. W. & Dillin, A. Opposing activities protect against age-onset proteotoxicity. *Science* **313,** 1604–1610 (2006).
7. Pinkston, J. M., Garigan, D., Hansen, M. & Kenyon, C. Mutations that increase the life span of *C. elegans* inhibit tumor growth. *Science* **313,** 971–975 (2006).
8. Hansen, M. & Kennedy, B. K. Does longer lifespan mean longer healthspan? *Trends Cell Biol.* **26,** 565–568 (2016).
9. Yin, J. A., Liu, X. J., Yuan, J., Jiang, J. & Cai, S. Q. Longevity manipulations differentially affect serotonin/dopamine level and behavioral deterioration in aging *Caenorhabditis elegans*. *J. Neurosci.* **34,** 3947–3958 (2014).
10. Yamazaki, D. *et al.* The *Drosophila* DCO mutation suppresses age-related memory impairment without affecting lifespan. *Nat. Neurosci.* **10,** 478–484 (2007).
11. Erikson, G. A. *et al.* Whole-genome sequencing of a healthy aging cohort. *Cell* **165,** 1002–1011 (2016).
12. Bansal, A., Zhu, L. J., Yen, K. & Tissenbaum, H. A. Uncoupling lifespan and healthspan in *Caenorhabditis elegans* longevity mutants. *Proc. Natl Acad. Sci. USA* **112,** E277–E286 (2015).
13. Guarente, L. Aging research—where do we stand and where are we going? *Cell* **159,** 15–19 (2014).
14. Whitehead, A. & Crawford, D. L. Variation within and among species in gene expression: raw material for evolution. *Mol. Ecol.* **15,** 1197–1211 (2006).
15. Anholt, R. R. H. & Mackay, T. F. C. Quantitative genetic analyses of complex behaviours in *Drosophila*. *Nat. Rev. Genet.* **5,** 838–849 (2004).
16. de Bono, M. & Bargmann, C. I. Natural variation in a neuropeptide Y receptor homolog modifies social behavior and food response in *C. elegans*. *Cell* **94,** 679–689 (1998).
17. Rockman, M. V., Skrovanek, S. S. & Kruglyak, L. Selection at linked sites shapes heritable phenotypic variation in *C. elegans*. *Science* **330,** 372–376 (2010).
18. Greene, J. S. *et al.* Balancing selection shapes density-dependent foraging behaviour. *Nature* **539,** 254–258 (2016).
19. Bendesky, A. & Bargmann, C. I. Genetic contributions to behavioural diversity at the gene-environment interface. *Nat. Rev. Genet.* **12,** 809–820 (2011).
20. Gloria-Soria, A. & Azevedo, R. B. *npr-1* regulates foraging and dispersal strategies in *Caenorhabditis elegans*. *Curr. Biol.* **18,** 1694–1699 (2008).
21. Loer, C. M. & Kenyon, C. J. Serotonin-deficient mutants and male mating behavior in the nematode *Caenorhabditis elegans*. *J. Neurosci.* **13,** 5407–5417 (1993).
22. Canaff, L., Bennett, H. P. & Hendy, G. N. Peptide hormone precursor processing: getting sorted? *Mol. Cell. Endocrinol.* **156,** 1–6 (1999).
23. Fares, H. & Greenwald, I. Genetic analysis of endocytosis in *Caenorhabditis elegans*: coelomocyte uptake defective mutants. *Genetics* **159,** 133–145 (2001).
24. Liu, A. M. *et al.* Gα 16/z chimeras efficiently link a wide range of G protein-coupled receptors to calcium mobilization. *J. Biomol. Screen.* **8,** 39–49 (2003).
25. Barr, M.M. & Garcia, L.R. in *WormBook* (ed. The *C. elegans* Research Community) https://dx.doi.org/10.1895/wormbook.1.78.1 (Wormbook, 2006).
26. Chatterjee, I. *et al.* Dramatic fertility decline in aging *C. elegans* males is associated with mating execution deficits rather than diminished sperm quality. *Exp. Gerontol.* **48,** 1156–1166 (2013).
27. Guo, X., Navetta, A., Gualberto, D. G. & Garcia, L. R. Behavioral decay in aging male C. elegans correlates with increased cell excitability. *Neurobiol. Aging* **33,** 1483.e5–1483.e23 (2012).
28. Lin, S. J., Defossez, P. A. & Guarente, L. Requirement of NAD and SIR2 for life-span extension by calorie restriction in *Saccharomyces cerevisiae*. *Science* **289,** 2126–2128 (2000).
29. Tissenbaum, H. A. & Guarente, L. Increased dosage of a *sir-2* gene extends lifespan in *Caenorhabditis elegans*. *Nature* **410,** 227–230 (2001).
30. Guo, X. & García, L. R. SIR-2.1 integrates metabolic homeostasis with the reproductive neuromuscular excitability in early aging male *Caenorhabditis elegans*. *eLife* **3,** e01730 (2014).
31. Mouchiroud, L. *et al.* The NAD+/sirtuin pathway modulates longevity through activation of mitochondrial UPR and FOXO signaling. *Cell* **154,** 430–441 (2013).
32. Imai, S. & Guarente, L. NAD+ and sirtuins in aging and disease. *Trends Cell Biol.* **24,** 464–471 (2014).
33. Wang, Y. & Hekimi, S. Mitochondrial dysfunction and longevity in animals: untangling the knot. *Science* **350,** 1204–1207 (2015).
34. Lin, Y. F. & Haynes, C. M. Metabolism and the UPR(mt). *Mol. Cell* **61,** 677–682 (2016).
35. Yoneda, T. *et al.* Compartment-specific perturbation of protein handling activates genes encoding mitochondrial chaperones. *J. Cell Sci.* **117,** 4055–4066 (2004).
36. Benedetti, C., Haynes, C. M., Yang, Y., Harding, H. P. & Ron, D. Ubiquitin-like protein 5 positively regulates chaperone gene expression in the mitochondrial unfolded protein response. *Genetics* **174,** 229–239 (2006).
37. Li, H. A new test for detecting recent positive selection that is free from the confounding impacts of demography. *Mol. Biol. Evol.* **28,** 365–375 (2011).
38. Andersen, E. C. *et al.* Chromosome-scale selective sweeps shape *Caenorhabditis elegans* genomic diversity. *Nat. Genet.* **44,** 285–290 (2012).
39. Hartigan, J. A. Minimum mutation fits to a given tree. *Biometrics* **29,** 53–65 (1973).
40. Williams, G. C. Pleiotropy, natural selection, and the evolution of senescence. *Evolution* **11,** 398–411 (1957).
41. Wong, A., Boutis, P. & Hekimi, S. Mutations in the *clk-1* gene of *Caenorhabditis elegans* affect developmental and behavioral timing. *Genetics* **139,** 1247–1259 (1995).
42. Gems, D. *et al.* Two pleiotropic classes of *daf-2* mutation affect larval arrest, adult behavior, reproduction and longevity in *Caenorhabditis elegans*. *Genetics* **150,** 129–155 (1998).
43. Jenkins, N. L., McColl, G. & Lithgow, G. J. Fitness cost of extended lifespan in *Caenorhabditis elegans*. *Proc. R. Soc. Lond. B* **271,** 2523–2526 (2004).
44. Crawford, D., Libina, N. & Kenyon, C. *Caenorhabditis elegans* integrates food and reproductive signals in lifespan determination. *Aging Cell* **6,** 715–721 (2007).
45. Botelho, M. & Cavadas, C. Neuropeptide Y: an anti-aging player? *Trends Neurosci.* **38,** 701–711 (2015).
46. Aveleira, C. A. *et al.* Neuropeptide Y stimulates autophagy in hypothalamic neurons. *Proc. Natl Acad. Sci. USA* **112,** E1642–E1651 (2015).
47. Kallio, J. *et al.* Altered intracellular processing and release of neuropeptide Y due to leucine 7 to proline 7 polymorphism in the signal peptide of preproneuropeptide Y in humans. *FASEB J.* **15,** 1242–1244 (2001).

Supplementary Information is available in the online version of the paper.

Acknowledgements We thank M.-M. Poo, X. Yu and D. Chen for critical reading of the manuscript; H.-W. Zhu and L.-S. Wang for mass spectrometry analysis; Y. H. Wong and J. Chu for providing the Gα16 and mRuby3 plasmids, respectively; Z. Chen and X. Bai for experimental assistance; and the Caenorhabditis Genetics Center for providing strains. This work was supported by the Strategic Priority Research Program of the Chinese Academy of Sciences (XDB 13000000) and the National Natural Science Foundation of China (31471149 and 81527901).

Author Contributions J.-A.Y. and G.G. performed most of the experiments. X.-J.L. performed male mating, locomotion and male retention assays. Z.-Q.H. and H.-P.L. performed population genetic analysis. K.L. carried out the endoplasmic reticulum fractionation assay. X.-L.K. conducted the male retention assay and helped to determine RGBA-1-2b. H.L., Y.-H.S., and W.-L.H. helped to conduct HPLC and mass spectrometry analysis of neuropeptides. S.-Q.C., J.-A.Y., and G.G. designed the study. S.-Q.C., J.-A.Y., G.G., and H.-P.L. analysed data and wrote the manuscript with input from all authors.

Author Information Reprints and permissions information is available at www.nature.com/reprints. The authors declare no competing financial interests. Readers are welcome to comment on the online version of the paper. Publisher's note: Springer Nature remains neutral with regard to jurisdictional claims in published maps and institutional affiliations. Correspondence and requests for materials should be addressed to S.-Q.C. (sqcai@ion.ac.cn).

Reviewer Information *Nature* thanks L. Bianchi, P. McGrath and the other anonymous reviewer(s) for their contribution to the peer review of this work.

METHODS

Worm strains and culture. Unless otherwise stated, all worms were cultivated on OP50-seeded nematode growth medium (NGM) plates at 20 °C. N2 (Bristol, UK), JU258 (Ribeiro Frio, Madeira), AB1 (Adelaide, Australia), AB3 (Adelaide, Australia), CB4854 (Altadena, USA), CB4856 (Hawaii, USA), RC301 (Freiburg, Germany), CB4857 (Claremont, USA), ED3049 (Ceres, South Africa), JU1400 (Sevilla, Spain), CB4932 (Taunton, UK), MY16 (Mecklenbeck, Germany), JU311 (Merlet, France), JU394 (Hermanville, France), JU1568 (Ivry-sur-Seine, France), JU1586 (Le Blanc, France), CX11262 (Los Angeles, USA), JT11398 (Lake Forest Park, USA), JU360 (Franconville, France), ED3017 (Edinburgh, UK), EG6699, *hsf-1(sy441)*, SJ4100, *sir-2.1(ok434)* and *unc-54(e190)* strains were obtained from the Caenorhabditis Genetics Center. *rgba-1(yfh081)*, *rgba-1(yfh084)*, *npr-28(yfh004)*, and *npr-28(yfh006)* worms were generated by CRISPR–Cas9-mediated genome editing. *rgba-1;npr-28* double mutant worms were generated by crossing *rgba-1(yfh081)* with *npr-28(yfh004)*. *rgba-1;sir-2.1* and *npr-28;sir-2.1* mutants were generated by crossing *sir-2.1(ok434)* with *rgba-1(yfh081)* and *npr-28(yfh004)*, respectively. *CB4856;rgba-1*^{3G4H} worms were obtained by changing the CB4856 3V4R *rgba-1* allele to the N2-type 3G4H *rgba-1* allele in the CB4856 genetic background. *N2;rgba-1*^{3V4H}, *N2;rgba-1*^{3G4R}, and *N2;rgba-1*^{3V4R} worms were generated by changing the 3G4H in *rgba-1* to 3V4H, 3G4R, or 3V4R, respectively, in the N2 genetic background. The *AB3;npr-28*^{N2} strain was generated by changing the AB3 *npr-28* allele to the N2-type *npr-28* allele in the AB3 genetic background, and *N2;npr-28*^{AB3} was generated by changing the N2 *npr-28* allele to the AB3-type *npr-28* allele in the N2 genetic background. The *AB3;npr-28*^{166L} strain was obtained by changing the 166M allele to the 166L *npr-28* allele in the AB3 genetic background, and *N2;npr-28*^{166M} worms were obtained by editing the 166L allele to the 166M *npr-28* allele in the N2 genetic background. The $P_{hsp\text{-}6}$*::gfp* transgenic strain SJ4100 was crossed with *rgba-1(yfh081)*, *npr-28(yfh004)*, *sir-2.1(ok434)*, *rgba-1;sir-2.1*, *npr-28;sir-2.1*, and *rgba-1;npr-28* worms to express $P_{hsp\text{-}6}$*::gfp* in these genetic backgrounds.

Molecular biology. The *rgba-1* gene with its 2.1-kb upstream promoter and 720-bp downstream 3′ UTR was amplified from N2 genomic DNA. To construct targeting plasmids for Mos1-meditated single-copy insertion, DNA fragments containing the *rgba-1* upstream promoter, the *ptr-10* promoter, the *mir-228* promoter, the *ges-1* promoter, or the *rab-3* promoter, followed by the *rgba-1* coding sequence and the *rgba-1* 3′ UTR were inserted into the pCFJ151 vector. To construct the $P_{rgba\text{-}1}$::GFP expression plasmid, the *rgba-1* promoter was ligated to the *gfp* coding sequence and the *rgba-1* 3′ UTR, and then inserted into the pPD95.75 vector. The $P_{npr\text{-}28}$::GFP reporter plasmid was generated by inserting a 4.1-kb upstream promoter of *npr-28* into pPD95.75, and the $P_{npr\text{-}28}$::npr-28 plasmid was generated by inserting a 2.4-kb DNA fragment containing full length *npr-28* DNA and 479-bp 3′ UTR into the $P_{npr\text{-}28}$::GFP plasmid. The $P_{tph\text{-}1}$::npr-28, $P_{dat\text{-}1}$::npr-28, and $P_{glr\text{-}1}$::npr-28 plasmids were generated by replacing the *npr-28* promoter with the *tph-1*, *dat-1*, or *glr-1* promoters, respectively, in the $P_{npr\text{-}28}$::npr-28 plasmid. $P_{ptr\text{-}10}$::Cre, $P_{mir\text{-}228}$::Cre, $P_{ges\text{-}1}$::Cre, and $P_{rab\text{-}3}$::Cre plasmids were generated by replacing the *eft-3* promoter in the pDD104 vector (Addgene)[48] with the *ptr-10* promoter, *mir-228* promoter, *ges-1* promoter, or *rab-3* promoter, respectively, and removing the *unc-119* gene in the pDD104 plasmid.

The $P_{hsp\text{-}16.2}$::rgba-1::mRuby3 plasmid was constructed by inserting a fusion of *rgba-1* and *mRuby3* (a gift from J. Chu[49]) coding sequence into the pPD49.83 vector (Addgene), and the $P_{hsp\text{-}16.2}$::mRuby3 plasmid was constructed by inserting *mRuby3* coding sequence into the pPD49.83 vector. The *hsf-1* cDNA was amplified from N2 transcripts and ligated to the *ptr-10* promoter and then inserted into the pPD95.75 vector to generate the $P_{ptr\text{-}10}$::hsf-1 plasmid.

For mammalian cell line expression of mCherry-fused signal peptide, 1–66 bp of *rgba-1* cDNA (encoding the signal peptide) was fused to *mCherry* cDNA and inserted into the pCIneo vector. *npr-28*^{166L} cDNA was amplified from N2 transcripts and ligated into the pCIneo vector to generate the npr-28^{166L} plasmid. The npr-28^{166M} plasmid was constructed by site-directed mutagenesis. *GCaMP6f* cDNA was inserted into the pCIneo vector to obtain the GCaMP6f-expressing plasmid.

All plasmids were verified by sequencing. Primers for constructing plasmids are as follows: *rgba-1* DNA: forward, 5′-ATGTTTGGGCACTCGACTTC-3′ and reverse, 5′-CTATCTACATCTACAGACAA-3′; *rgba-1* promoter: forward, 5′-CCCAAGTTGCCTGTAATGAG-3′ and reverse, 5′-TTTCCAACTTTGTTCTGAAGTTCGTAC-3′; *npr-28* promoter: forward, 5′-GACACTATGCGTCCGTGAGC-3′ and reverse, 5′-AGTAGAATAACTGACAAGTCGTG-3′; *npr-28* DNA: forward, 5′-ATGTCGACAATGACTATCAGTTCC-3′ and reverse, 5′-CTACAACCATTCGACAGACG-3′; *npr-28* cDNA: forward, 5′-ATGTCGACAATGACTATCAG-3′ and reverse, 5′-CTACAACCATTCGACAGACG-3′; *tph-1* promoter: forward, 5′-TCGGTGGTCTTCCCGCTTG-3′ and reverse, 5′-ATGATTGAAGAGAGCAATGC-3′; *dat-1* promoter: forward, 5′-AATCTTCTCATCAGGGCACC-3′ and reverse, 5′-GGCTAAAAATTGTTGAG-3′; *glr-1* promoter: forward, 5′-CTGTAGCCGGTATGCACTGATA-3′ and reverse, 5′-TGTGAATGTGTCAGATTGGGTGCC-3′; *ptr-10* promoter: forward, 5′-CATCTTACGGAATAACCCTG-3′ and reverse, 5′-CTCTGGAACTTTATTTTAGC-3′; *mir-228* promoter: forward, 5′-TGCAATGCGGGAAGAGACGA-3′ and reverse, 5′-AGGAAAATGTCTCGCCAAAG-3′; *ges-1* promoter: forward, 5′-TCCGCCACTTAACCTAAATT-3′ and reverse, 5′-CTGAATTCAAAGATAAGATATGTAATAG-3′; *rab-3* promoter: forward, 5′-ATCTTCAGATGGGAGCAGTGG-3′ and reverse, 5′-CTGAAAATAGGGCTACTGTA-3′; *GCaMP6f* cDNA: forward, 5′-ATGGGTTCTCATCATCATCATC-3′ and reverse, 5′-TCACTTCGCTGTCATCATTTG-3′; *mRuby3* cDNA: forward, 5′-ATGGTGTCTAAGGGCGAAGA-3′ and reverse, 5′-TTACTTGTACAGCTCGTCCA-3′; *hsf-1* cDNA: forward, 5′-ATGCAGCCAACAGGGAATCAAATAC-3′ and reverse, 5′-TTAAACCAAATTAGGATCCGATG-3′.

Generation of transgenic animals. All transgenic strains were generated by microinjection of the respective plasmid using standard protocol[50], and at least two independent lines of each transformation were used for experiments. The deletion of *rgba-1* in specific tissues was performed by Cre–*LoxP*-mediated recombination. The *LoxP* sites were inserted in both termini of the *rgba-1* gene by CRISPR–Cas9-mediated genome editing in N2 worms to generate a *LoxP-rgba-1-LoxP* strain (named *rgba-1*$^{flox/flox}$). We expressed Cre recombinase in glial cells (with *ptr-10* promoter or *mir-228* promoter[51,52]), neurons (with *rab-3* promoter[53]), or intestinal cells (with *ges-1* promoter[54]) to conditionally delete *rgba-1* in *rgba-1*$^{flox/flox}$ worms. The specific expression of N2-type NPR-28 in serotonergic, dopaminergic, and motor (or inter-) neurons of *npr-28*-null worms was performed by fusing N2-type *npr-28* with *tph-1*, *dat-1*, and *glr-1* promoters[55–57], respectively, and injecting them into *npr-28*-null worms. The detailed information about transgenic strains is as follows: SQC0017, *yfhIx0017* ($P_{bas\text{-}1}$::bas-1::GFP at 50 ng μl^{-1}); SQC0009, SQC0010, *yfhEx0009, yfhEx0010* ($P_{rgba\text{-}1}$::GFP at 100 ng μl^{-1}; rol-6(su1006) at 10 ng μl^{-1}); SQC0011, SQC0012, *rgba-1*$^{flox/flox}$*;yfhEx0011, yfhEx0012* ($P_{ptr\text{-}10}$::Cre at 50 ng μl^{-1}; $P_{myo\text{-}2}$::mCherry at 2.5 ng μl^{-1}); SQC0013, SQC0014, *rgba-1*$^{flox/flox}$*; yfhEx0013, yfhEx0014* ($P_{mir\text{-}228}$::Cre at 50 ng μl^{-1}; $P_{myo\text{-}2}$::mCherry at 2.5 ng μl^{-1}); SQC0021, SQC0022, *rgba-1*$^{flox/flox}$*;yfhEx0021, yfhEx0022* ($P_{ges\text{-}1}$::Cre at 50 ng μl^{-1}; $P_{myo\text{-}2}$::mCherry at 2.5 ng μl^{-1}); SQC0023, SQC0024, *rgba-1*$^{flox/flox}$*;yfhEx0023, yfhEx0024* ($P_{rab\text{-}3}$::Cre at 50 ng μl^{-1}; $P_{myo\text{-}2}$::mCherry at 2.5 ng μl^{-1}); SQC0025, SQC0026, *yfhEx0025, yfhEx0026* ($P_{npr\text{-}28}$::GFP at 30 ng μl^{-1}; rol-6(su1006) at 10 ng μl^{-1}); SQC0027, SQC0028, *yfhEx0027, yfhEx0028* ($P_{npr\text{-}28}$::GFP at 30 ng μl^{-1}; $P_{dat\text{-}1}$::mCherry at 30 ng μl^{-1}; rol-6(su1006) at 10 ng μl^{-1}); SQC0029, SQC0030, *yfhEx0029, yfhEx0030* ($P_{npr\text{-}28}$::GFP at 30 ng μl^{-1}; $P_{tph\text{-}1}$::mCherry at 30 ng μl^{-1}; rol-6(su1006) at 10 ng μl^{-1}); SQC0031, SQC0032, *yfhEx0031, yfhEx0032* ($P_{npr\text{-}28}$::GFP at 30 ng μl^{-1}; $P_{glr\text{-}1}$::mCherry at 30 ng μl^{-1}; rol-6(su1006) at 10 ng μl^{-1}); SQC0035, SQC0036, *npr-28(yfh004);yfhEx0035, yfhEx0036* ($P_{dat\text{-}1}$::npr-28 at 30 ng μl^{-1}; $P_{myo\text{-}2}$::mCherry at 2.5 ng μl^{-1}); SQC0037, SQC0038, *npr-28(yfh004); yfhEx0037, yfhEx0038* ($P_{tph\text{-}1}$::npr-28 at 30 ng μl^{-1}; $P_{myo\text{-}2}$::mCherry at 2.5 ng μl^{-1}); SQC0039, SQC0040, *npr-28(yfh004);yfhEx0039, yfhEx0040* ($P_{glr\text{-}1}$::npr-28 at 30 ng μl^{-1}; $P_{myo\text{-}2}$::mCherry at 2.5 ng μl^{-1}); SQC0041, *SQC0002;yfhSi0041* (*MosSCI* Cbr-unc-119(+)) *II; unc-119(ed3) III*; SQC0043, *SQC0002;yfhSi0043* (*MosSCI* $P_{rgba\text{-}1}$::rgba-1::3′ UTR + Cbr-unc-119(+)) *II; unc-119(ed3) III*; SQC0045, *rgba-1 (yfh081);yfhSi0045* (*MosSCI* Cbr-unc-119(+)) *II; unc-119(ed3) III*; SQC0046, *rgba-1(yfh081);yfhSi0046* (*MosSCI* $P_{ptr\text{-}10}$::rgba-1::3′ UTR + Cbr-unc-119(+)) *II; unc-119(ed3) III; SQC0047, rgba-1(yfh081);yfhSi0047* (*MosSCI* $P_{mir\text{-}228}$::rgba-1::3′ UTR + Cbr-unc-119(+)) *II; unc-119(ed3) III*; SQC0048, *rgba-1 (yfh081);yfhSi0048* (*MosSCI* $P_{rab\text{-}3}$::rgba-1::3′ UTR + Cbr-unc-119(+)) *II; unc-119(ed3) III*; SQC0049, *rgba-1(yfh081);yfhSi0049* (*MosSCI* $P_{ges\text{-}1}$::rgba-1::3′ UTR + Cbr-unc-119(+)) *II; unc-119(ed3) III*; SQC0051, *hsf-1(sy441);yfhEx0051* ($P_{hsp\text{-}16.2}$::mRuby3 at 80 ng μl^{-1}; $P_{ptr\text{-}10}$::hsf-1 at 20 ng μl^{-1}; $P_{unc\text{-}122}$::GFP at 20 ng μl^{-1}; rol-16(su1006) at 20 ng μl^{-1}); SQC0052, *hsf-1(sy441);yfhEx0052* ($P_{hsp\text{-}16.2}$::rgba-1^{3G4H}::mRuby3 at 80 ng μl^{-1}; $P_{ptr\text{-}10}$::hsf-1 at 20 ng μl^{-1}; $P_{unc\text{-}122}$::GFP at 20 ng μl^{-1}; rol-16(su1006) at 20 ng μl^{-1}); SQC0053, *hsf-1(sy441);yfhEx0053* ($P_{hsp\text{-}16.2}$::rgba-1^{3V4H}::mRuby3 at 80 ng μl^{-1}; $P_{ptr\text{-}10}$::hsf-1 at 20 ng μl^{-1}; $P_{unc\text{-}122}$::GFP at 20 ng μl^{-1}; rol-16(su1006) at 20 ng μl^{-1}); SQC0054, *hsf-1(sy441);yfhEx0054* ($P_{hsp\text{-}16.2}$::rgba-1^{3G4R}::mRuby3 at 80 ng μl^{-1}; $P_{ptr\text{-}10}$::hsf-1 at 20 ng μl^{-1}; $P_{unc\text{-}122}$::GFP at 20 ng μl^{-1}; rol-16(su1006) at 20 ng μl^{-1}); SQC0055, *hsf-1(sy441);yfhEx0055* ($P_{hsp\text{-}16.2}$::rgba-1^{3V4R}::mRuby3 at 80 ng μl^{-1}; $P_{ptr\text{-}10}$::hsf-1 at 20 ng μl^{-1}; $P_{unc\text{-}122}$::GFP at 20 ng μl^{-1}; rol-16(su1006) at 20 ng μl^{-1}).

Gene mapping. Whole-genome sequencing of SQC0002 was accomplished on Illumina platform (HiSeq 2000/2500) and data were analysed by CloudMap (https://usegalaxy.org)[58]. For the fosmid rescue assay, WRM0634cE01, WRM066aA04, WRM0618bA07, WRM064bB01, WRM064aE08, WRM0623cD03, WRM0633dC02, WRM0639cH05, WRM0619aF07, and WRM0610aA01 were injected individually into SQC0002 worms at 5 ng μl^{-1} together with 2.5 ng μl^{-1} $P_{myo\text{-}2}$::mCherry. Genes in fosmid WRM0633dC02 were cloned and injected individually into SQC0002 at 5 ng μl^{-1} with $P_{myo\text{-}2}$::mCherry at 2.5 ng μl^{-1}. In each transgenic line, BAS-1::GFP expression was detected by fluorescent imaging using a Nikon A1R confocal microscope.

Generation of single-copy insertion lines. Mos1-mediated single-copy insertions of transgenes were performed as described[59]. The *ttTi5605mos* insertion site was introduced into the genomes of SQC0002 and *rgba-1(yfh081)* worms by crossing them with EG6699 (*ttTi5605 II; unc-119(ed3) III*). A mixture of P_{rgba-1}::rgba-1-containing targeting vector (at 5 ng μl^{-1}), pJL43.1 (at 50 ng μl^{-1}), pCFJ90 (at 2.5 ng μl^{-1}), pCFJ104 (at 5 ng μl^{-1}), and pGH8 (at 5 ng μl^{-1}) was injected to generate SQC0002 worms with a single-copy insertion of *rgba-1*. Single-copy insertions of P_{ptr-10}::rgba-1, $P_{mir-228}$::rgba-1, P_{rab-3}::rgba-1, or P_{ges-1}::rgba-1 were performed in *rgba-1(yfh081)* worms with the *ttTi5605mos* insertion site.

CRISPR–Cas9-mediated genome editing. CRISPR–Cas9-mediated genome editing was carried out as described[48]. Single-guide RNA (sgRNA) targeting sequences were individually cloned into the pDD162 vector (Addgene) by site-directed mutagenesis. sgRNAs used for generating *rgba-1*- and *npr-28*-null worms are as follows: *rgba-1* sgRNA targeting sequence, 5′-TAAAGATCCTTGGTATGAC-3′; *npr-28* sgRNA1 targeting sequence, 5′-AGTAGGCCTTACAAGACAG-3′; *npr-28* sgRNA2 targeting sequence, 5′-GTGCTGACTGCACTGTCTG-3′. Detailed information for *rgba-1* and *npr-28* mutant alleles is as follows: *rgba-1(yfh081)* is a mutant strain with a 18-bp deletion in *rgba-1*. This mutation deletes six amino acid residues and causes K-to-E transition at the 30th amino acid residue. *rgba-1(yfh084)* is a mutant strain with a 4-bp deletion in *rgba-1*. This mutation causes a reading frame shift. *npr-28(yfh004)* is a mutant strain with a 1-bp insertion followed by a 196-bp deletion in *npr-28*. This mutation truncates the predicted second and third transmembrane domains. *npr-28(yfh006)* is a mutant strain with a 202-bp deletion in *npr-28*. This mutation causes a reading frame shift.

For genome editing in *rgba-1* of CB4856 and N2 worms, we used two sgRNAs targeting two loci of *rgba-1* to induce a DNA double-strand break. A pPD95.75 plasmid, containing 1.3-kb left and 1.3-kb right homology arms of genome-editing sites from N2 genomic DNA, was used as a repair donor. sgRNAs used for this experiment are as follows: sgRNA1 targeting sequence for genome editing in *rgba-1* SNP sites, 5′-AATAAAGCCAAAAGACAGA-3′; sgRNA2 targeting sequence for genome editing in *rgba-1* SNP sites, 5′-CTCGACTTCCTTCTGTCTTT-3′.

To generate *rgba-1*$^{flox/flox}$ worms, we inserted the *LoxP* sequence at 9 bp upstream and 337 bp downstream from the *rgba-1* start codon, in the same orientation. sgRNAs used for knock-in of *LoxP* sites are as follows: sgRNA1 targeting sequence for knock-in of *LoxP* sites, 5′-ACGAACTTCAGAACAAAGT-3′; sgRNA2 targeting sequence for knock-in of *LoxP* sites, 5′-ATAGATAATCTTGTTTTAA-3′.

For genome editing in *npr-28* of AB3 and N2 worms, a repair template with approximately 1-kb left and right homology arms of genome editing sites was amplified by PCR from N2 genomic DNA, and cloned into the pPD95.75 vector. sgRNAs used are as follows: sgRNA1 targeting sequence for genome editing in *npr-28* SNP sites, 5′-TAACCAGTACAACGTGGGA-3′; sgRNA2 targeting sequence for genome editing in *npr-28* SNP sites, 5′-GCAGTTGCAGAAGAGGTGC-3′.

For all CRISPR–Cas9-mediated genome editing assays, Cas9 target sites in donor plasmids were synonymously mutated to avoid Cas9-mediated cleavage of repair templates. sgRNA (50 ng μl^{-1}) and donor plasmids (10 ng μl^{-1}) were co-injected with 10 ng μl^{-1} *rol-6(su1006)*. Genome editing was confirmed by DNA sequencing.

Male mating. Male mating efficiency was assessed as described[9]. L4 males were picked out and cultured at a density of approximately 40 virgin males per 60-mm plate. Two males of each genotype and two young N2 hermaphrodites were transferred to a 35-mm NGM plate with 5-mm-diameter OP50 lawn, and males were removed 24 h later. We scored about 20 mating plates in each experiment. Successful mating was scored when more than 3 male progeny existed in the mating plate. Male mating efficiency was obtained by calculating the percentage of mating plates with successful mating.

Male mating steps were analysed as described[60], with the following modifications. In brief, roughly 15 young *unc-54 (e190)* hermaphrodites were transferred to a 35-mm NGM plate with 2-mm-diameter OP50 lawn and allowed to adapt for 1 h before the experiment began. One virgin male was placed on the plate, and mating behaviour was recorded when the tail of this male came into contact with a hermaphrodite. The recording was sustained for 3 min. Response to hermaphrodites was measured by counting the number of hermaphrodites that came into contact with the tail of the male worm, before mating. Turning efficiency was scored as the number of males with no turning defect divided by the total number of tested males. Successful vulva locating was defined as a situation in which the male stopped backing for more than 10 s, when his tail was located in the vulva of a hermaphrodite. Vulva location efficiency was calculated by dividing the number of successful vulva locations by the total number of vulva contacts. For ejaculation assay, a virgin male and several *unc-54(e190)* hermaphrodites were transferred to the plate with 2-mm-diameter OP50 lawn, and recording began when the male initiated spicule insertion and continued for 5 min. Unsuccessful ejaculation was defined as those situations in which little or no sperm was transferred to the uterus of the hermaphrodite. Sperm transfer efficiency was calculated by dividing the number of males that successfully ejaculated by the number of males that successfully performed spicule insertion.

Male retention. Male retention assay was conducted on 9-cm-diameter Petri plates (seeded with 20 μl OP50 the night before examination) as described[61]. In each experiment, approximately 10–15 virgin males were placed individually onto the centre of the OP50 lawn with two young *unc-54(e190)* hermaphrodites. A male was considered as a 'leaver' when it reached a distance that was over 3 cm from the food patch. The proportion of leavers was scored at seven time points during 24 h at 20 °C.

Locomotion assay. Synchronized young adult hermaphrodites were transferred to OP50-seeded NGM plates (at a density of no more than 80 animals per 60-mm plate) with 6 μM floxuridine. The locomotion of worms was recorded every other day, from day 2 to day 14 of adulthood, using a microscope with an OLYMPUS DP72 CCD camera. About 20 animals were placed in a dispersed fashion across a 35-mm NGM plate without OP50 and their spontaneous movement was tracked for 1 min. Locomotion speed was quantified by analysing the first 300 frames of each recording using wrMTrck (ImageJ).

Pharyngeal pumping. The pharyngeal pumping rate assay was conducted as described previously[9]. Synchronized hermaphrodites were raised on OP50-seeded plates and allowed to adapt for 10 min at room temperature (approximately 20 °C), and then the pharyngeal pumping rate of roughly 15 animals was counted under a dissection microscope.

Lifespan assay. Lifespan was measured following previous protocols[9]. In brief, approximately 90 young adult hermaphrodites were transferred onto OP50-seeded plates (roughly 30 animals per plate) containing 6 μM floxuridine, and dead worms were counted every other day until all worms were dead. Worms that crawled out of the plates were not counted.

Peptide isolation. Total neuropeptides were isolated from about 2 ml of a mixture of N2 males and hermaphrodites according to published procedures[60,62], with minor modifications. In brief, after the evaporation of methanol, the residual aqueous fraction was re-extracted with hexanes to remove lipids, centrifuged at 13,000*g* for 15 min at 4 °C, and then subjected to HPLC (Agilent 1260 with a G4212B DAD) on a Thermo Hypersil Gold 3 μm analytical C18 column (150 × 4.6 mm) for fraction separation. The column was equilibrated for 30 min with 2% CH_3CN and 1% formic acid, and then peptides were eluted in a 4-step linear gradient over 70 min: 20 min at 2–22% CH_3CN and 1% formic acid; 30 min at 22–37% CH_3CN and 1% formic acid; 10 min at 37–50% CH_3CN and 1% formic acid; and 10 min at 50–100% CH_3CN and 1% formic acid (at 20 °C, flow rate 0.6 ml min^{-1}, wave length 215 nm). Synthetic putative peptides (Chinapeptides) were run in parallel under the same conditions. Fractions around the putative candidates were collected and condensed for mass spectrometry analysis.

Mass spectrometry. Tandem mass spectrometry was performed using a Q Exactive hybrid quadrupole-Orbitrap mass spectrometer (Thermo Fisher Scientific) coupled to the UltiMate 3000 RSLCnano system (Thermo Fisher Scientific). HPLC fractions were lyophilized and re-dissolved in 20 μl solvent (2% CH_3CN and 0.1% formic acid in ddH_2O). A five microlitre sample was loaded on a C18 PepMap100 pre-column (300 μm × 5 mm, 5 μm, Thermo Fisher Scientific) and eluted on an Acclaim PepMap 100 analytical column (75 μm × 15 cm, C18, 3 μm, Thermo Fisher Scientific) with a 60 min gradient. CH_3CN and H_2O (2:98, v/v) with 0.1% formic acid, and CH_3CN and H_2O (4:1, v/v) with 0.1% formic acid, were used as mobile phases A and B, respectively. The loading buffer was the same as mobile phase A. The gradient was 5 min at 10% mobile phase B, a 33 min linear gradient of 10%–40% mobile phase B, and a 4 min linear gradient of 40%–95% mobile phase B. After washing the column for 3 min with 95% mobile phase B, the buffer was decreased to 10% mobile phase B within 1 min and the column was reconditioned at the initial gradient for 14 min. The column temperature was 35 °C. The flow rates through the trap column and analytical column were 3 μl min^{-1} and 0.3 μl min^{-1}, respectively. Tandem mass spectrometry experiments were operated in the data-dependent mode with automatic switching between mass spectrometry and tandem mass spectrometry scans, using a top-10 method. Data analysis was performed using Thermo Proteome Discoverer software (Thermo Fisher Scientific) with a mass range of 350–2,000 *m*/*z* (mass to charge ratio).

HPLC and mass spectrometry quantification of RGBA-1-2b. Total neuropeptides from an approximately 5-ml pellet of N2 or CB4856 worms at day 1 of adulthood were extracted, and subjected to HPLC for separation. RGBA-1-2b-containing fractions were collected and condensed for mass spectrometry analysis. RGBA-1-2b was quantified using an Orbitrap Fusion Lumos Tribrid mass spectrometer and Xcalibur 4.0 software (Thermo Fisher Scientific). A gradient running from 10 pg μl^{-1} to 10 ng μl^{-1} of synthesized RGBA-1-2b (Chinapeptides) was run under the same conditions and used as a linear reference for quantification. The level of RGBA-1-2b was normalized to the total proteins of the sample.

Immunocytochemistry. When they reached 80–90% confluence, HEK293T cells were transfected with 0.5 μg mCherry-fused signal peptide plasmid, using

Lipofectamine 2000 (Invitrogen). Cells were split 6 h later and then plated onto a cover slide coated with poly-D-lysine, in a new dish. Roughly 24 h after transfection, cells were fixed with 4% paraformaldehyde (Sigma–Aldrich), and then permeablized with 0.25% Triton X-100. Cells were blocked with 1% BSA and then incubated with anti-calnexin (Abcam, ab22595) followed by Alexa Fluor 488-conjugated secondary antibodies (Invitrogen, A-21206). Cellular localization of the signal peptide was examined by monitoring mCherry distribution. Normal endoplasmic reticulum localization was defined as mCherry co-localized with the endoplasmic reticulum marker protein calnexin; severe mislocalization of mCherry was defined as mCherry distributed in the cytoplasm; and mild mislocalization of mCherry was defined as mCherry localized both in the endoplasmic reticulum and the remaining components of the cytoplasm. The experiment was repeated four times. Cells were randomly chosen and the experimenter was blind to the allele type when conducting data analysis.

Endoplasmic reticulum fractionation. Endoplasmic reticulum fractionation was performed using the endoplasmic reticulum isolation kit (Sigma, ER0100), with modifications. Cultured HEK293T cells were grown in 10-cm dishes. Twenty-four hours after transfection with 10 μg mCherry-fused RGBA-1 signal peptide plasmids, cells were collected by scraping into the cell fractionation buffer (sucrose 0.25 mM, NaCl 140 mM, EDTA 1 mM, and Tris-HCl 20 mM, pH 8.0, supplemented with a protease inhibitor mixture) and lysed in a Dounce homogenizer with ten passes. The nuclei were removed by centrifugation at 700*g* for 10 min and the post-nuclear supernatants were then layered onto a linear gradient of 5–30% iodixanol reagent in the cell fractionation buffer, and centrifuged at 200,000*g* for 6 h at 4 °C. After centrifugation, twelve fractions were collected from the top to the bottom of the gradient, and then subjected to SDS–PAGE. Immunoblot analyses were performed using antibodies against calnexin (Abcam, ab22595) and mCherry (Earthox, E022110-01).

RGBA-1 secretion assay. The secretion assay was performed according to previous studies[23,63], with modifications. In brief, HSF-1 was specifically expressed in glial cells by the driver of the *ptr-10* promoter in *hsf-1*-null (*hsf-1(sy441)*) worms. After heat shock, HSF-1 binds to the heat-shock promoter $P_{hsp\text{-}16.2}$, which drives the expression of RGBA-1::mRuby3. Secreted RGBA-1::mRuby3 enters the pseudocoelom and can be taken up by coelomocytes. The fluorescence intensity of young adult transgenic worms was measured after four cycles of a 1-h heat shock at 34 °C followed by a 30-min recovery at 20 °C. The ratio of secreted and retained RGBA-1::mRuby3 was calculated by dividing the fluorescence intensity of mRuby3 in two anterior coelomocytes (ccPR and ccAR) by the fluorescence intensity of mRuby3 in sheath and socket cells near the nerve ring.

Calcium imaging. COS-7 cells were used for NPR-28 functional assays. Two micrograms *npr-28*^{166M} or *npr-28*^{166L}, together with 1 μg Gα16 (a gift from Y. H. Wong[24]) and 0.5 μg GCaMP6f plasmids, were transfected in COS-7 cells using Lipofectamine 2000 (Invitrogen). Cells were split 6 h after transfection, and then plated onto a cover slide coated with poly-D-lysine, in a new dish. Calcium imaging was performed approximately 40 h after transfection. Cells transfected with empty vector and the Gα16 plasmid were used as a negative control. Transfected cells on cover slides were moved to a 24-well plate containing 0.5 ml DMEM. The calcium signal was monitored for 2 min before application of synthetic peptides, and recorded for 3–5 min after peptide administration, using a 20× magnification object at 1 Hz in a Nikon A1R confocal imaging system. For the dose–response assay, NPR-28^{166M} or NPR-28^{166L} were expressed together with Gα16 and GCaMP6f in COS-7 cells. The EC_{50} of RGBA-1-2b for activating NPR-28 was calculated using Prism (GraphPad Software) nonlinear regression.

RNA isolation and real-time PCR. Total RNA from 800 to 1,000 synchronized males at day 5 of adulthood was isolated, and 600 ng RNA was used as a template to generate cDNA. Real-time PCR was performed on a Roche LightCycler 480 system using SYBR Green (Takara). The *pmp-3* gene was used as an internal reference. Primers used for real-time PCR were the same as previously reported[30,64].

RNA interference. RNAi was performed as previously described, without floxuridine[9]. For screening downstream effectors of RGBA-1, L4 $P_{bas\text{-}1}$*::bas-1::gfp* hermaphrodites, with expression of SID-1 (driven by the *unc-119* promoter) to enhance neuronal RNAi efficiency[65], were transferred to plates seeded with bacteria expressing double-stranded RNAs that target neuropeptide receptor genes. Four days later, BAS-1::GFP fluorescence of the F1 progeny was measured.

For the *ubl-5* RNAi assay, L4 $P_{hsp\text{-}6}$*::gfp* transgenic hermaphrodites were transferred to plates seeded with bacteria that expressed *ubl-5* or control double-stranded RNAs, and the $P_{hsp\text{-}6}$::GFP fluorescence of F1 progeny was examined four days later. GFP fluorescence was normalized to average fluorescence intensity of N2 worms. Roughly 50 males at day 1 of adulthood were transferred to plates seeded with bacteria that expressed *ubl-5* double-stranded RNAs. Four or six days later, male mating efficiency was examined on OP50-seeded plates. For CB4856 and AB3 males, one male was allowed to mate with two young adult N2 hermaphrodites for 12 h. Empty vector was used as control in all experiments. RNAi clones are from the *C. elegans* RNAi Collection (Ahringer)[66] and were confirmed by sequencing. Sequences for *npr-28* and *ubl-5* RNAi constructs are included in the Supplementary Information.

Population genetics. We downloaded the DNA polymorphism data of a 20-kb region centred on *rgba-1* and *npr-28*, from the *C. elegans* Natural Diversity Resource (www.elegansvariation.org). The phylogenetic tree of these polymorphisms was reconstructed and naturally rooted by the unweighted pair group method with arithmetic mean (UPGMA)[67]. The genetic distance was calculated by a maximum composite likelihood method[68] and the tree reconstruction was performed by MEGA 7 (ref. 39). The neighbour joining method[69] was also applied; the topologies of the un-rooted neighbour joining trees were generally similar to the topologies of UPGMA trees. Consequently, the tree construction methods should not affect ancestral allele inferences. Homologues of NPR-28 were obtained by protein blast search on the NCBI website (https://blast.ncbi.nlm.nih.gov/Blast.cgi), and their alignment was used to reconstruct the neighbour joining tree. To detect selective sweep, Tajima's *D* values were calculated[70,71]. When performing the unbalanced test in detecting selective sweep, the size of the maximum and minimum basal branches is denoted by ψ and $n - \psi$, respectively (n = sample size). The *P* value of the test is given by $2(n - \psi)$ divided by $(n - 1)$ (ref. 37).

Data reporting and statistics. No statistical methods were used to predetermine sample size. The sample size in our experiments was determined from related previous analyses in the literature. All behavioural and lifespan experiments were performed at room temperature (roughly 20 °C), and were repeated on at least three days. The experimenters were blind to the genotype or double-stranded RNA treatment. For lifespan assays, healthy young adult worms were used and worms that crawled off the plate were not included in the data. For behaviour analysis, healthy L4 worms were picked and raised on plates with bacteria lawn, and they were chosen for behavioural assays at a range of ages, without bias, to ensure randomization. For the male mating assay, mating plates with males or hermaphrodites that crawled out the plate during the assay were not included in the analysis. For immunocytochemical assays, HEK293T cells were randomly chosen for analysis, and the experimenter who performed data analysis was blind to the allele types. For the calcium imaging assay in COS-7 cells, the experimenter was not blind to the allele types. HEK293T (Catalogue number SCSP-502) and COS-7 (Catalogue number SCSP-508) cell lines were ordered from the cell bank of the Chinese Academy of Sciences. These cell lines have been validated by the cell bank of the Chinese Academy of Sciences using the short tandem repeat profiling method, and we did not test for mycoplasma contamination.

For most statistical comparisons, one-way analysis of variance with Dunnett's correction test was used for multiple comparisons and two-sided Student's *t* test was used for comparisons between two sets of data. Two-way ANOVA was used in Fig. 1a. Two-sided log-rank test was used in Fig. 1d and Extended Data Fig. 7h. Fisher's exact test was used in Extended Data Fig. 7c, e. Kruskal–Wallis with Dunn's test was used for Supplementary Table 1. The normality of the data was tested with the Shapiro–Wilk normality test. We used the Brown–Forsythe test to examine differences in variance between groups. Statistical analyses were performed using the Graphpad 7.0 software and all these tests have been noted in figure legends. The precise *P* values for figures and tables are provided in the statistical test result section of Supplementary Information. Sample sizes for Fig. 1b, c, Fig. 3c, Extended Data Fig. 7f, g, and Extended Data Table 1 are included in the sample size section of the Supplementary Information.

Data availability. Source Data for each figure are available in the online version of the paper. All other data are available from the corresponding author upon reasonable request.

48. Dickinson, D. J., Ward, J. D., Reiner, D. J. & Goldstein, B. Engineering the *Caenorhabditis elegans* genome using Cas9-triggered homologous recombination. *Nat. Methods* **10,** 1028–1034 (2013).
49. Bajar, B. T. *et al.* Improving brightness and photostability of green and red fluorescent proteins for live cell imaging and FRET reporting. *Sci. Rep.* **6,** 20889 (2016).
50. Hope, I. A. *C. elegans: A Practical Approach* (Oxford Univ. Press, 1999).
51. Yoshimura, S., Murray, J. I., Lu, Y., Waterston, R. H. & Shaham, S. *mls-2* and *vab-3* control glia development, *hlh-17*/Olig expression and glia-dependent neurite extension in *C. elegans*. *Development* **135,** 2263–2275 (2008).
52. Wallace, S. W., Singhvi, A., Liang, Y., Lu, Y. & Shaham, S. PROS-1/Prospero is a major regulator of the glia-specific secretome controlling sensory-neuron shape and function in *C. elegans*. *Cell Reports* **15,** 550–562 (2016).
53. Tursun, B., Patel, T., Kratsios, P. & Hobert, O. Direct conversion of *C. elegans* germ cells into specific neuron types. *Science* **331,** 304–308 (2011).
54. Egan, C. R. *et al.* A gut-to-pharynx/tail switch in embryonic expression of the *Caenorhabditis elegans ges-1* gene centers on two GATA sequences. *Dev. Biol.* **170,** 397–419 (1995).

55. Maricq, A. V., Peckol, E., Driscoll, M. & Bargmann, C. I. Mechanosensory signalling in *C. elegans* mediated by the GLR-1 glutamate receptor. *Nature* **378,** 78–81 (1995).
56. Sze, J. Y., Victor, M., Loer, C., Shi, Y. & Ruvkun, G. Food and metabolic signalling defects in a *Caenorhabditis elegans* serotonin-synthesis mutant. *Nature* **403,** 560–564 (2000).
57. Nass, R., Hall, D. H., Miller, D. M., III & Blakely, R. D. Neurotoxin-induced degeneration of dopamine neurons in *Caenorhabditis elegans*. *Proc. Natl Acad. Sci. USA* **99,** 3264–3269 (2002).
58. Doitsidou, M., Poole, R. J., Sarin, S., Bigelow, H. & Hobert, O. *C. elegans* mutant identification with a one-step whole-genome-sequencing and SNP mapping strategy. *PLoS One* **5,** e15435 (2010).
59. Frøkjær-Jensen, C. *et al.* Single-copy insertion of transgenes in *Caenorhabditis elegans*. *Nat. Genet.* **40,** 1375–1383 (2008).
60. Garrison, J. L. *et al.* Oxytocin/vasopressin-related peptides have an ancient role in reproductive behavior. *Science* **338,** 540–543 (2012).
61. Lipton, J., Kleemann, G., Ghosh, R., Lints, R. & Emmons, S. W. Mate searching in *Caenorhabditis elegans*: a genetic model for sex drive in a simple invertebrate. *J. Neurosci.* **24,** 7427–7434 (2004).
62. Husson, S. J. *et al.* Approaches to identify endogenous peptides in the soil nematode *Caenorhabditis elegans*. *Methods Mol. Biol.* **615,** 29–47 (2010).
63. Bacaj, T. & Shaham, S. Temporal control of cell-specific transgene expression in *Caenorhabditis elegans*. *Genetics* **176,** 2651–2655 (2007).
64. Merkwirth, C. *et al.* Two conserved histone demethylases regulate mitochondrial stress-induced longevity. *Cell* **165,** 1209–1223 (2016).
65. Calixto, A., Chelur, D., Topalidou, I., Chen, X. & Chalfie, M. Enhanced neuronal RNAi in *C. elegans* using SID-1. *Nat. Methods* **7,** 554–559 (2010).
66. Fraser, A. G. *et al.* Functional genomic analysis of *C. elegans* chromosome I by systematic RNA interference. *Nature* **408,** 325–330 (2000).
67. Sneath, P. H. A. & Sokal, R. R. *Numerical Taxonomy; The Principles and Practice of Numerical Classification* (W. H. Freeman, 1973).
68. Tamura, K., Nei, M. & Kumar, S. Prospects for inferring very large phylogenies by using the neighbor-joining method. *Proc. Natl Acad. Sci. USA* **101,** 11030–11035 (2004).
69. Saitou, N. & Nei, M. The neighbor-joining method: a new method for reconstructing phylogenetic trees. *Mol. Biol. Evol.* **4,** 406–425 (1987).
70. Excoffier, L., Laval, G. & Schneider, S. Arlequin (version 3.0): an integrated software package for population genetics data analysis. *Evol. Bioinform. Online* **1,** 47–50 (2007).
71. Tajima, F. Statistical method for testing the neutral mutation hypothesis by DNA polymorphism. *Genetics* **123,** 585–595 (1989).

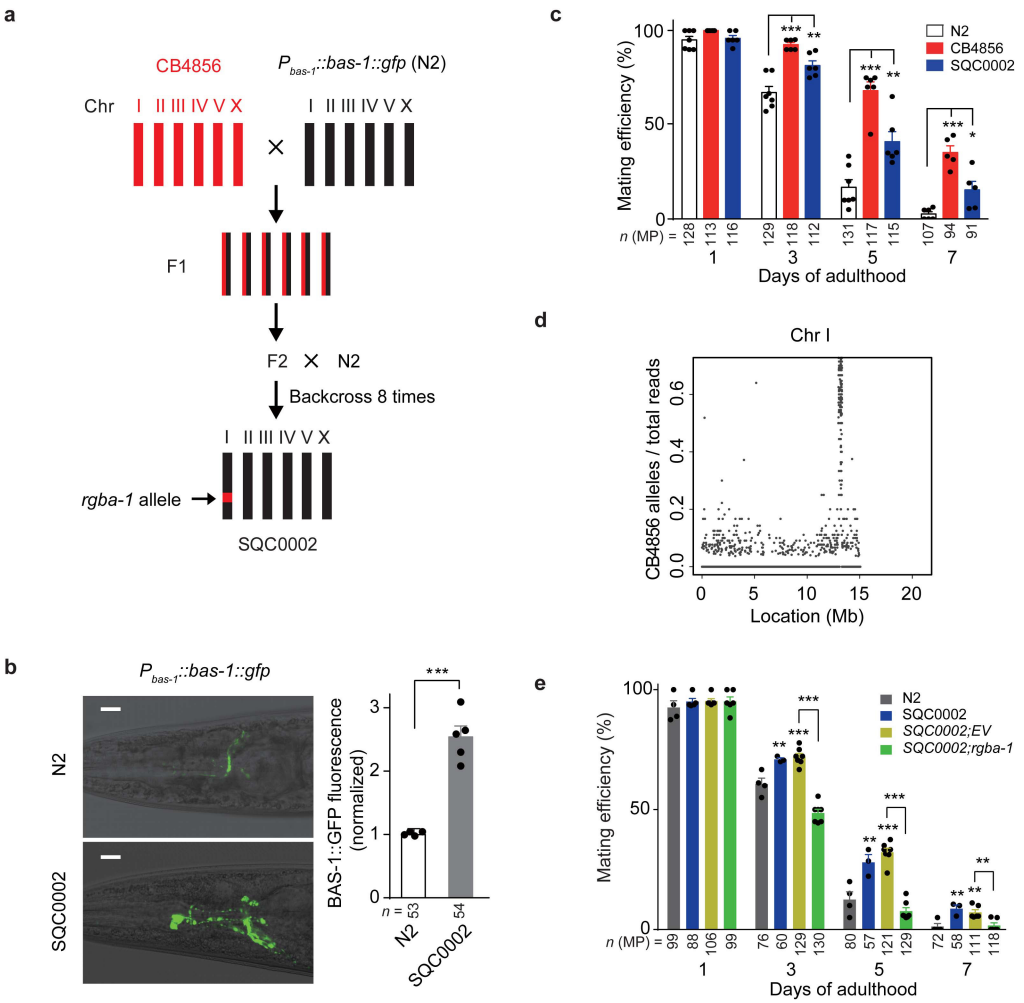

Extended Data Figure 1 | Cloning of *rgba-1*. **a**, Schematic illustration of generation of SQC0002 strain. CB4856 was crossed with P_{bas-1}::*bas-1*::*gfp* transgenic worms (with N2 genetic background), and about a quarter of aged F2 progeny showed an elevated level of BAS-1::GFP expression. The F2 progeny with high expression levels of BAS-1 were backcrossed with N2 worms eight times; the resulting strain was named SQC0002. **b**, Left, expression of BAS-1::GFP in SQC0002 and N2 worms at day 9 of adulthood. Scale bar, 10 μm. Representative of $n = 5$ independent experiments. Right, quantification of BAS-1::GFP fluorescence intensity. GFP fluorescence was normalized to average fluorescence intensity of age-matched N2 worms. **c**, Mating efficiency of SQC0002, CB4856, and N2 males at a range of ages. **d**, Whole-genome sequencing of SQC0002 worms identified a 328-kb region in chromosome I that possessed enriched CB4856 alleles. **e**, Age-dependent changes in mating efficiency in N2, SQC0002, and SQC0002 males with single-copy transgene of empty vector (*SQC0002;EV*) or *rgba-1* (*SQC0002;rgba-1*). All data shown are mean ± s.e.m. $*P < 0.05$, $**P < 0.01$, $***P < 0.001$ (**b**, two-sided *t* test; **c**, **e**, ANOVA with Dunnett's test). For **b**, **c** and **e**, each data point represents the result of one independent experiment. The numbers of tested worms (**b**) and mating plates (**c**, **e**) are shown beneath the bars.

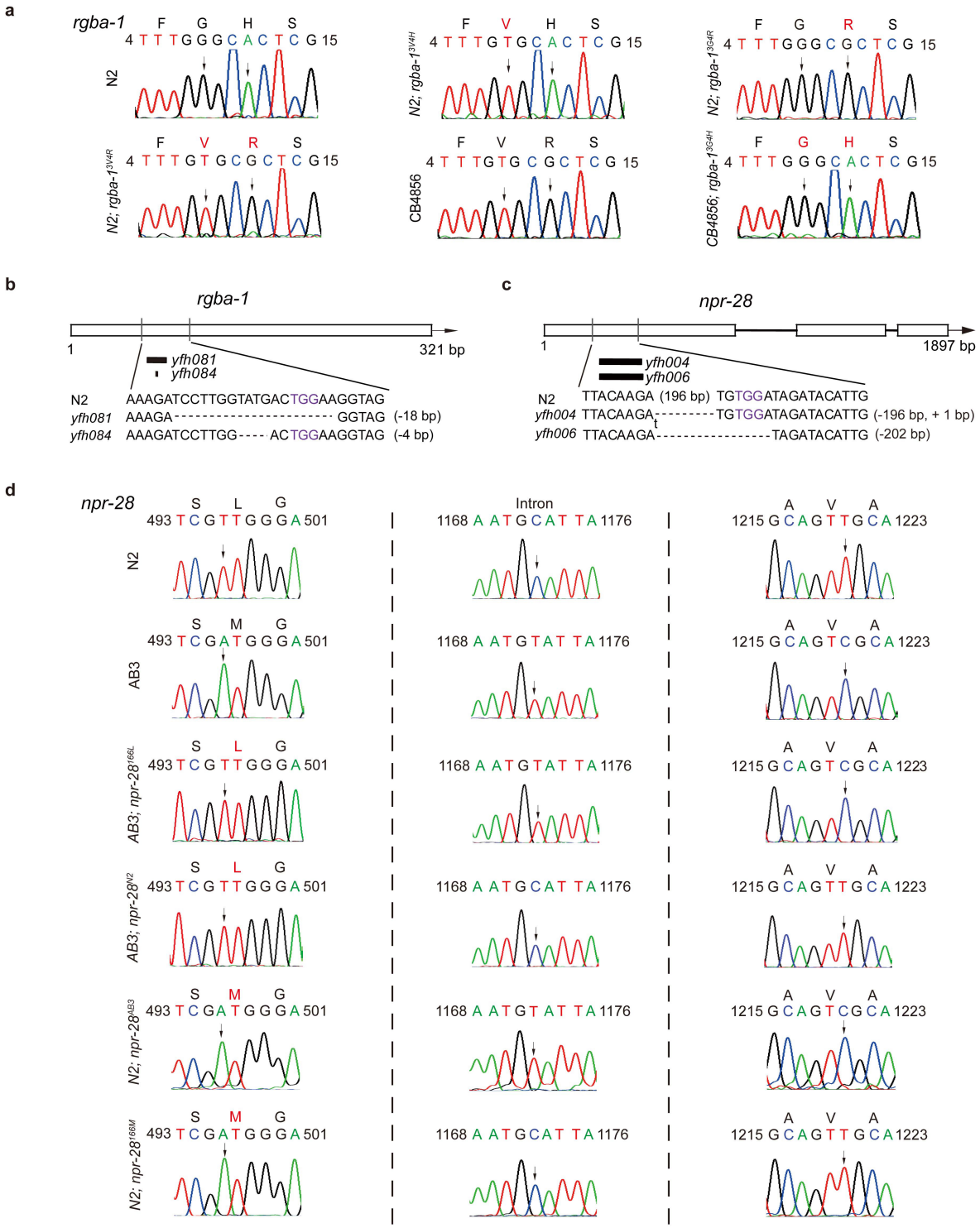

Extended Data Figure 2 | CRISPR–Cas9-mediated genome editing in *rgba-1* and *npr-28* genes. a, Sequence confirmation of *N2;rgba-1*^{3V4H}, *N2;rgba-1*^{3G4R}, *N2;rgba-1*^{3V4R}, and *CB4856;rgba-1*^{3G4H} worms. The *N2;rgba-1*^{3V4H}, *N2;rgba-1*^{3G4R}, and *N2;rgba-1*^{3V4R} worms were generated by converting the 3G4H *rgba-1* allele to 3V4H, 3G4R, and 3V4R, respectively, in N2 worms. The *CB4856;rgba-1*^{3G4H} worms were generated by changing the 3V4R *rgba-1* allele to 3G4H in CB4856 worms. Black arrows indicate SNP sites. **b**, **c**, Schematic illustrations of molecular details of *rgba-1* (**b**) and *npr-28* (**c**) mutations. Three nucleotides highlighted in purple represent the protospacer-adjacent motif. **d**, Sequence confirmation of *AB3;npr-28*^{N2}, *AB3;npr-28*^{166L}, *N2;npr-28*^{AB3}, and *N2;npr-28*^{166M} worms. The *AB3;npr-28*^{166L} and *AB3;npr-28*^{N2} worms were generated by changing the *npr-28* allele to the 166L and N2-type *npr-28* allele, respectively, in AB3 worms. *N2;npr-28*^{166M} and *N2;npr-28*^{AB3} worms were generated by changing the *npr-28* allele to the 166M and the AB3-type *npr-28* allele, respectively, in N2 worms. Black arrows indicate SNP sites.

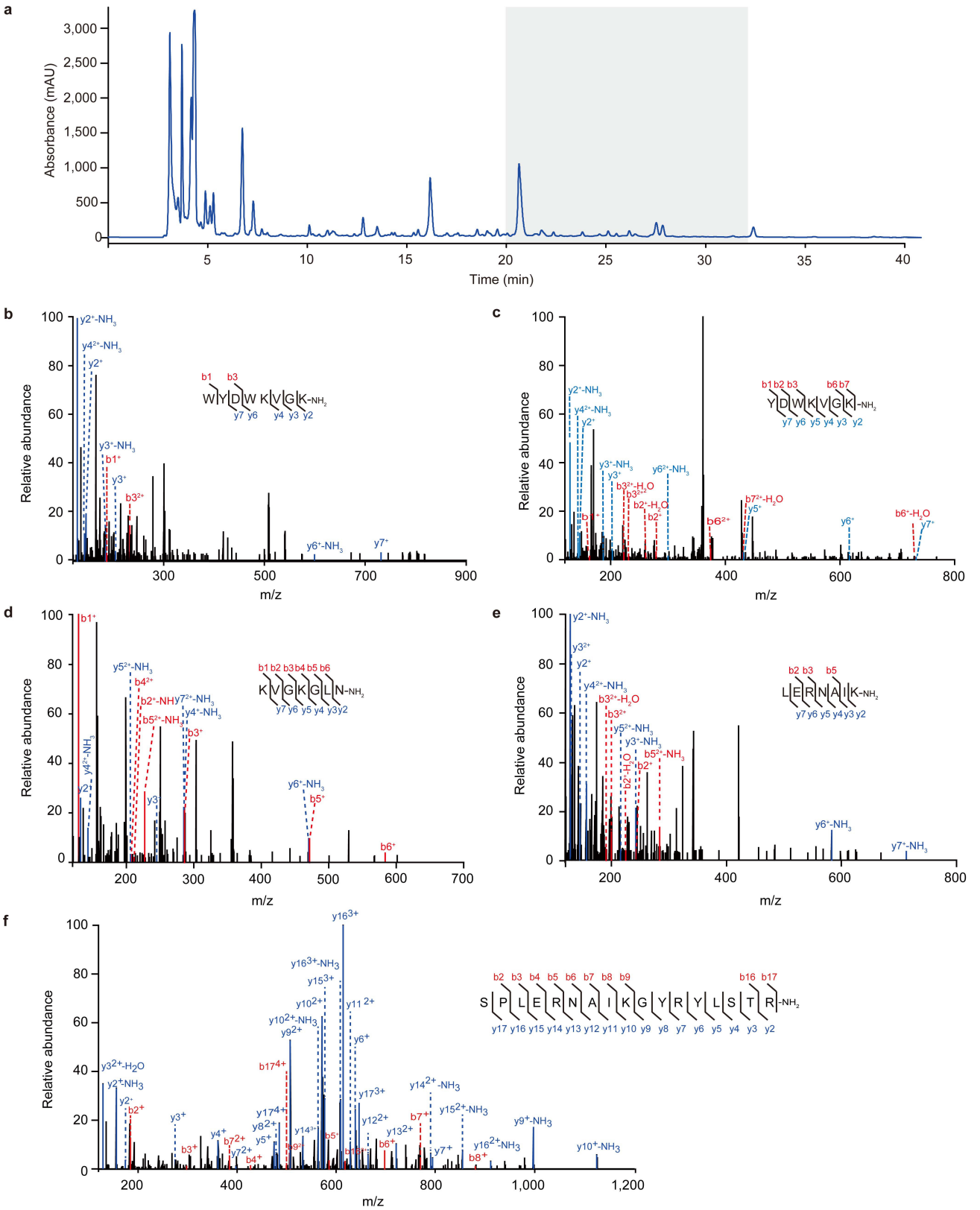

Extended Data Figure 3 | Isolation and characterization of RGBA-1-derived peptides. a, Separation of N2 worm neuropeptides by HPLC. Total neuropeptides were isolated from the mixture of N2 males and hermaphrodites. Grey bar indicates fractions selected for further analysis. mAU, milli-absorbance unit. **b**–**f**, Tandem mass spectrometry spectrum of RGBA-1-derived peptides. Peptide sequence was confirmed by higher-energy collisional dissociation fragmentation; y-type and b-type ions are shown in the spectrum.

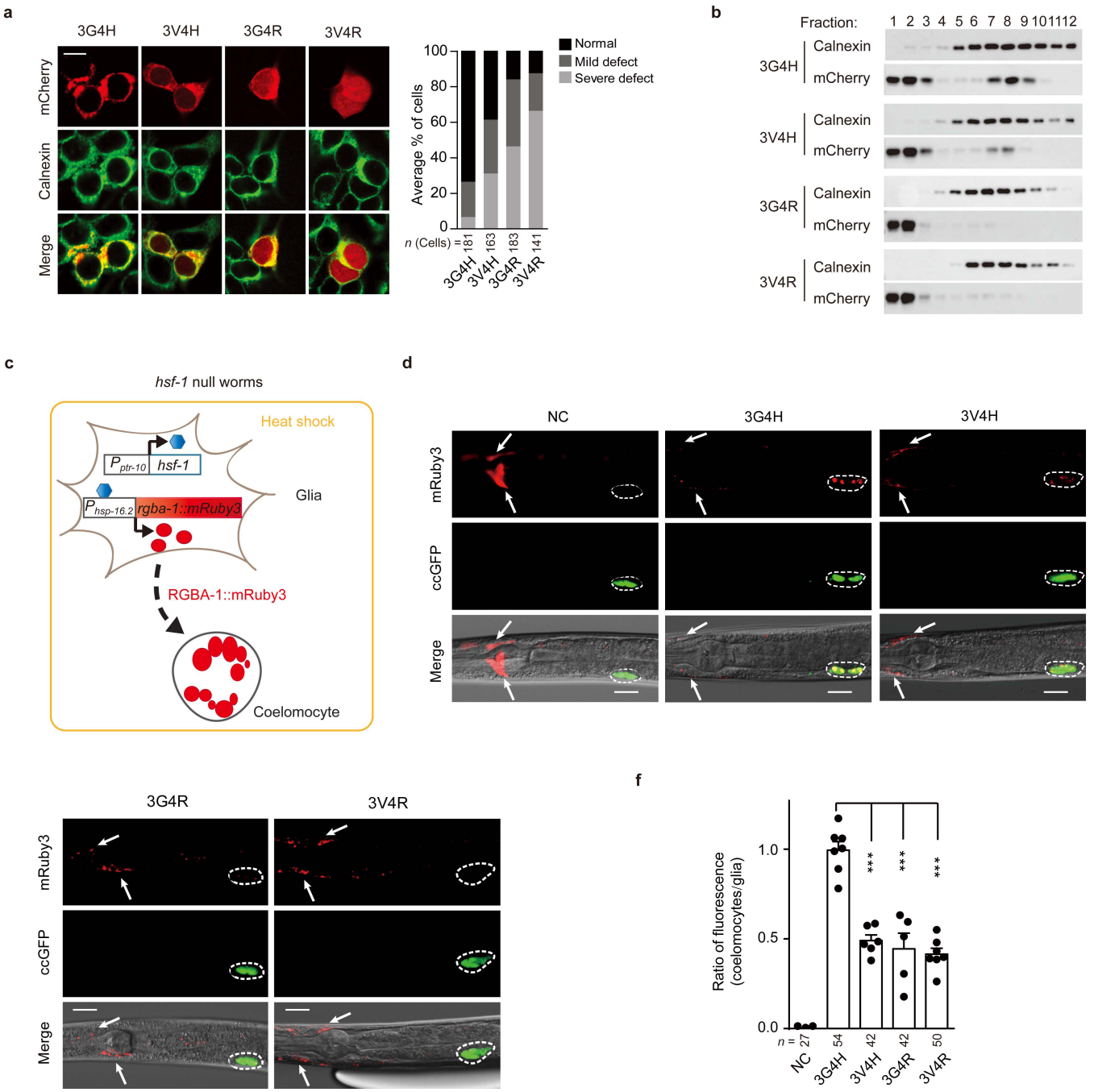

Extended Data Figure 4 | Polymorphisms in the signal peptide affect RGBA-1 production. a, Left, representative images show co-localization of mCherry-fused RGBA-1 signal peptides with an endoplasmic reticulum marker protein calnexin, in HEK293T cells. Scale bar, 10 μm; Right, quantitative analysis of cells with normal, mildly defective, and severely impaired endoplasmic reticulum-localization of RGBA-1 signal peptides. **b**, Cell fractionation and western blot analyses of mCherry-fused RGBA-1 signal peptides. Cell fractionation was performed by density gradient centrifugation. The endoplasmic reticulum fractions were indicated by the presence of calnexin using anti-calnexin, and mCherry-fused RGBA-1 signal peptides were visualized by anti-mCherry. For gel source data, see Supplementary Fig. 1a. **c**, Schematic of the RGBA-1::mRuby3 secretion assay. **d**, **e**, Images showing RGBA-1-fused mRuby3 fluorescence in glia and coelomocytes (labelled by $P_{unc-122}$::GFP reporter, ccGFP). The expression of $P_{hsp-16.2}$::mRuby3 was used as negative control (NC). Arrows point to glial cells and dashed circles indicate coelomocytes. Scale bar, 20 μm. **f**, Quantitative analysis of the ratio of RGBA-1::mRuby3 fluorescence in coelomocytes to that in glial cells. Each data point represents the result of one independent experiment. The total number of tested worms is shown beneath the bar. Data shown are mean ± s.e.m. ***$P < 0.001$ (ANOVA with Dunnett's test). For **a** and **b**, $n = 4$ (**a**) or 3 (**b**) independent experiments.

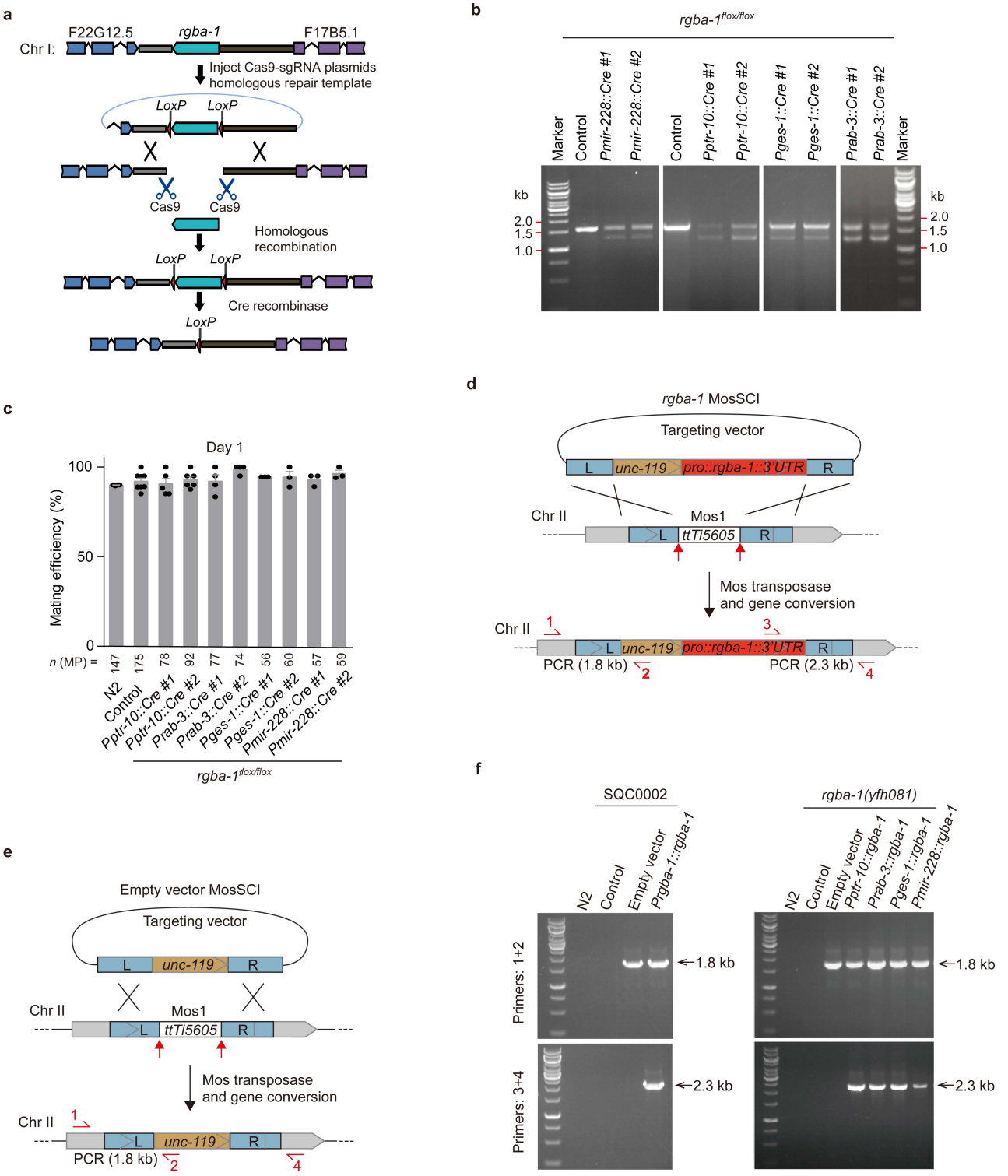

Extended Data Figure 5 | Cre–*LoxP*-mediated recombination and Mos1-mediated single-copy insertion of *rgba-1* gene. a, Schematic representation of Cre–*LoxP*-mediated recombination of *rgba-1* gene. **b**, The cleavage of *rgba-1* in various tissues was verified by PCR. **c**, Mating efficiency of N2 males at day 1 of adulthood with conditional deletion of *rgba-1* in glial cells (*rgba-1*$^{flox/flox}$;P_{ptr-10}::*Cre* or *rgba-1*$^{flox/flox}$;$P_{mir-228}$::*Cre*), neurons (*rgba-1*$^{flox/flox}$;P_{rab-3}::*Cre*), or intestinal cells (*rgba-1*$^{flox/flox}$;P_{ges-1}::*Cre*). Data shown are mean ± s.e.m. Each data point represents the result of one independent experiment. **d**, **e**, Schematic representations of Mos1-mediated single-copy insertion of *rgba-1* (**d**) or empty vector (**e**). **f**, PCR validation of Mos1-mediated insertion of *rgba-1*. For **b** and **f**, $n = 2$ (**b**) or 3 (**f**) independent experiments. For gel source data, see Supplementary Fig. 1b.

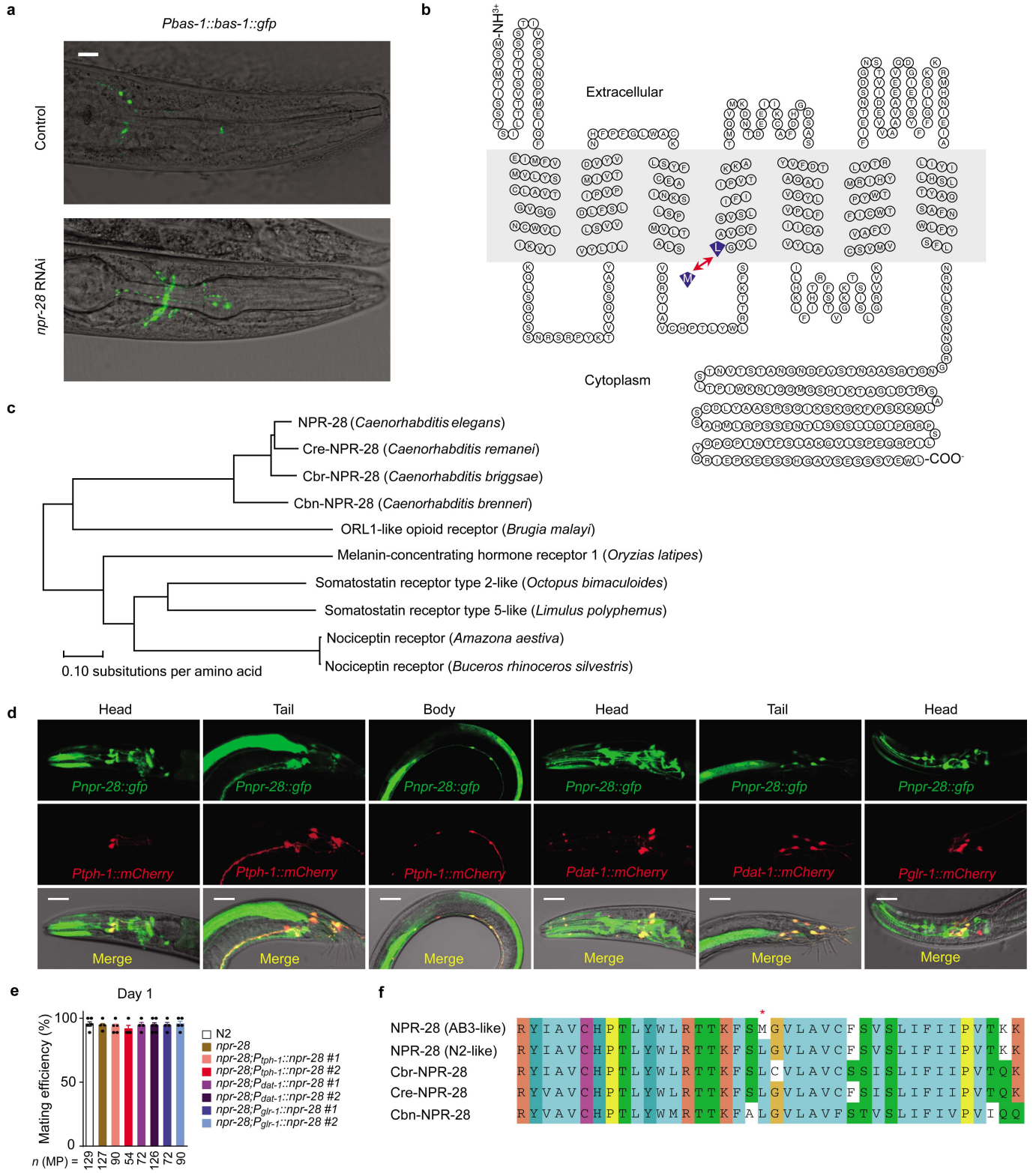

Extended Data Figure 6 | RNAi screening for BAS-1 regulators identified *npr-28*. **a**, Expression of BAS-1::GFP in N2 worms fed with bacteria that express control or *npr-28* double-stranded RNAs. Scale bar, 10 μm. Representative of $n = 3$ independent experiments. **b**, Predicted transmembrane topology of NPR-28. The variable residue is highlighted in blue. Alignment of NPR-28 with human somatostatin receptor 5 was used for prediction. **c**, A phylogenetic tree of NPR-28. **d**, Expression of NPR-28 in serotonergic, dopaminergic, and motor (or inter-) neurons of N2 males. Serotonergic, dopaminergic, and motor (or inter-) neurons were identified by expression of P_{tph-1}::mCherry, P_{dat-1}::mCherry, and P_{glr-1}::mCherry, respectively. Scale bar, 20 μm. Representative of $n = 2$ independent experiments. **e**, Mating efficiency of *npr-28*-null males selectively expressing N2-type NPR-28 in serotonergic, dopaminergic, and motor (or inter-) neurons at day 1 of adulthood. Two independent transgenic lines per genotype were examined. Data shown are mean ± s.e.m. Each data point represents the result of one independent experiment. **f**, Alignment of a 30-amino-acid sequence centred at the variable 166th residue from NPR-28 of *C. elegans* and its *Caenorhabditis briggsae*, *Caenorhadbitis remanei*, and *Caenorhabditis brenneri* homologues. The red asterisk indicates the variation site in wild strains of *C. elegans*.

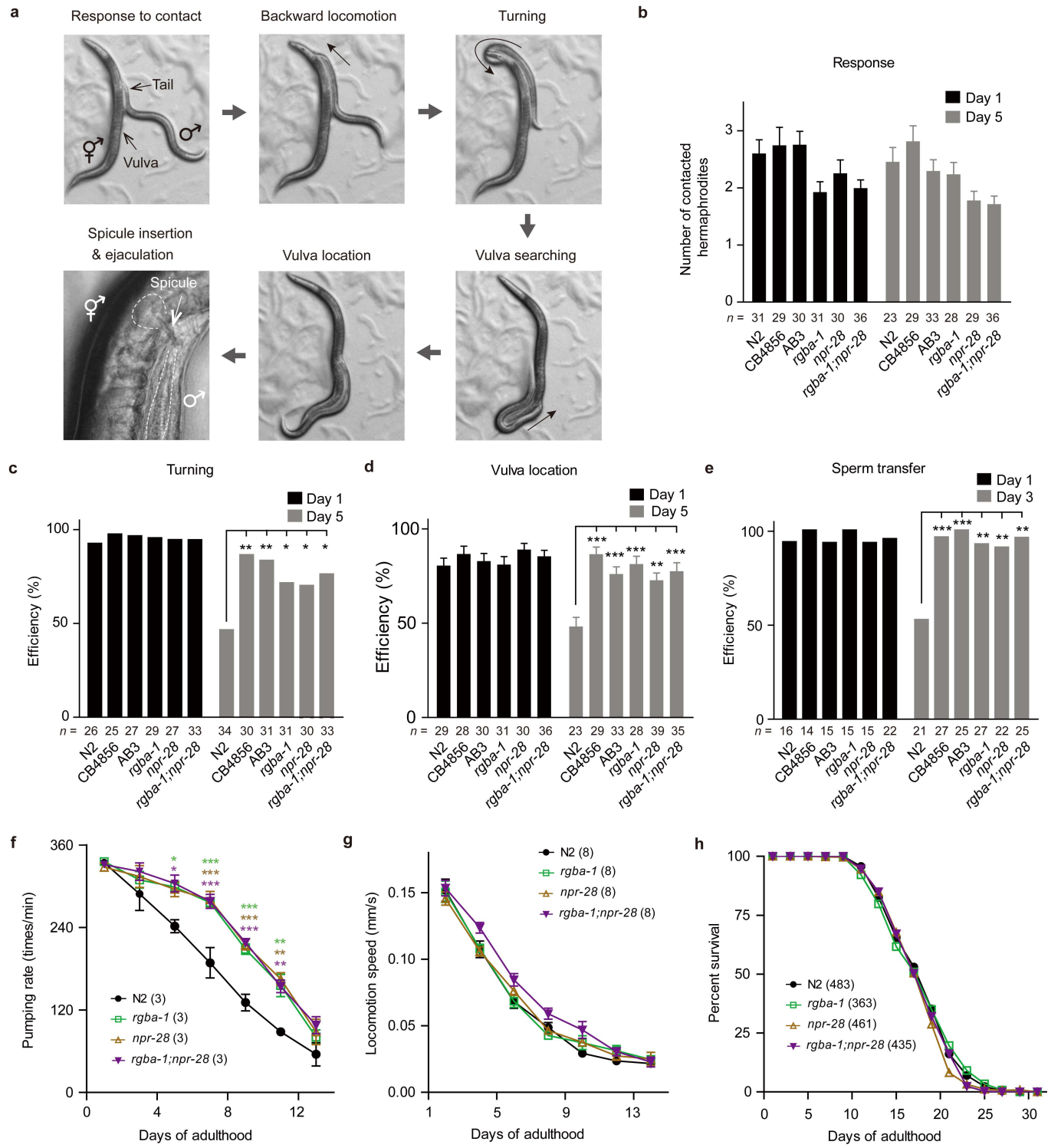

Extended Data Figure 7 | RGBA-1 and NPR-28 regulate deterioration of multiple behaviours. a, *C. elegans* male mating steps. Dashed lines indicate the transport of sperm. **b**, Number of hermaphrodites contacted by a male before mating initiation. **c**, **d**, Turning (**c**) and vulva location (**d**) efficiency of males during mating. **e**, The efficiency of sperm transfer. For **b**–**e**, the numbers of tested males are shown beneath the bars. **f**, **g**, Age-dependent changes in pharyngeal pumping rate (**f**) and locomotion speed (**g**) in N2, *rgba-1*, *npr-28*, and *rgba-1;npr-28* mutant worms. The numbers of independent experiments are indicated in parentheses. **h**, Lifespan curves of N2, *rgba-1*, *npr-28*, and *rgba-1;npr-28* mutant worms. The numbers of tested hermaphrodites are indicated in parentheses. Data shown in **b**, **d**, **f** and **g** are mean ± s.e.m., and in **c**, **e**, and **h** represent the sum of animals in three (**c**, **e**) or four (**h**) independent experiments. $*P < 0.05$, $**P < 0.01$, $***P < 0.001$ (**b**, **d**, **f**, and **g**, ANOVA with Dunnett's test; **c**, **e**, Fisher's exact test; **h**, two-sided log-rank test).

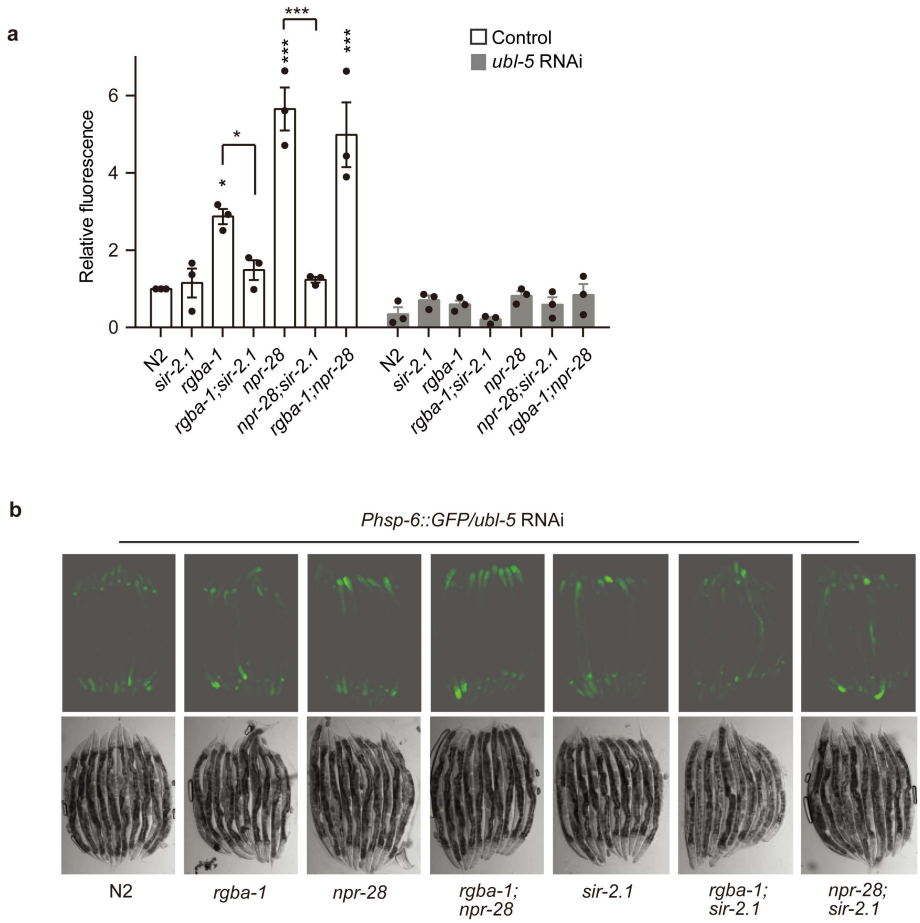

Extended Data Figure 8 | The effect of *ubl-5* RNAi on UPR^{mt} in *rgba-1* and *npr-28* worms. a, Quantification of UPR^{mt} by measuring the fluorescence intensity of P_{hsp-6}::GFP. $n = 3$ repeated experiments. Each data point represents the result of one independent experiment. Data shown are mean ± s.e.m. $^{*}P < 0.05$, $^{***}P < 0.001$. (ANOVA with Dunnett's test). **b**, Fluorescent images of worms expressing the UPR^{mt} reporter P_{hsp-6}::GFP in the presence of *ubl-5* RNAi. Representative of $n = 3$ repeated experiments.

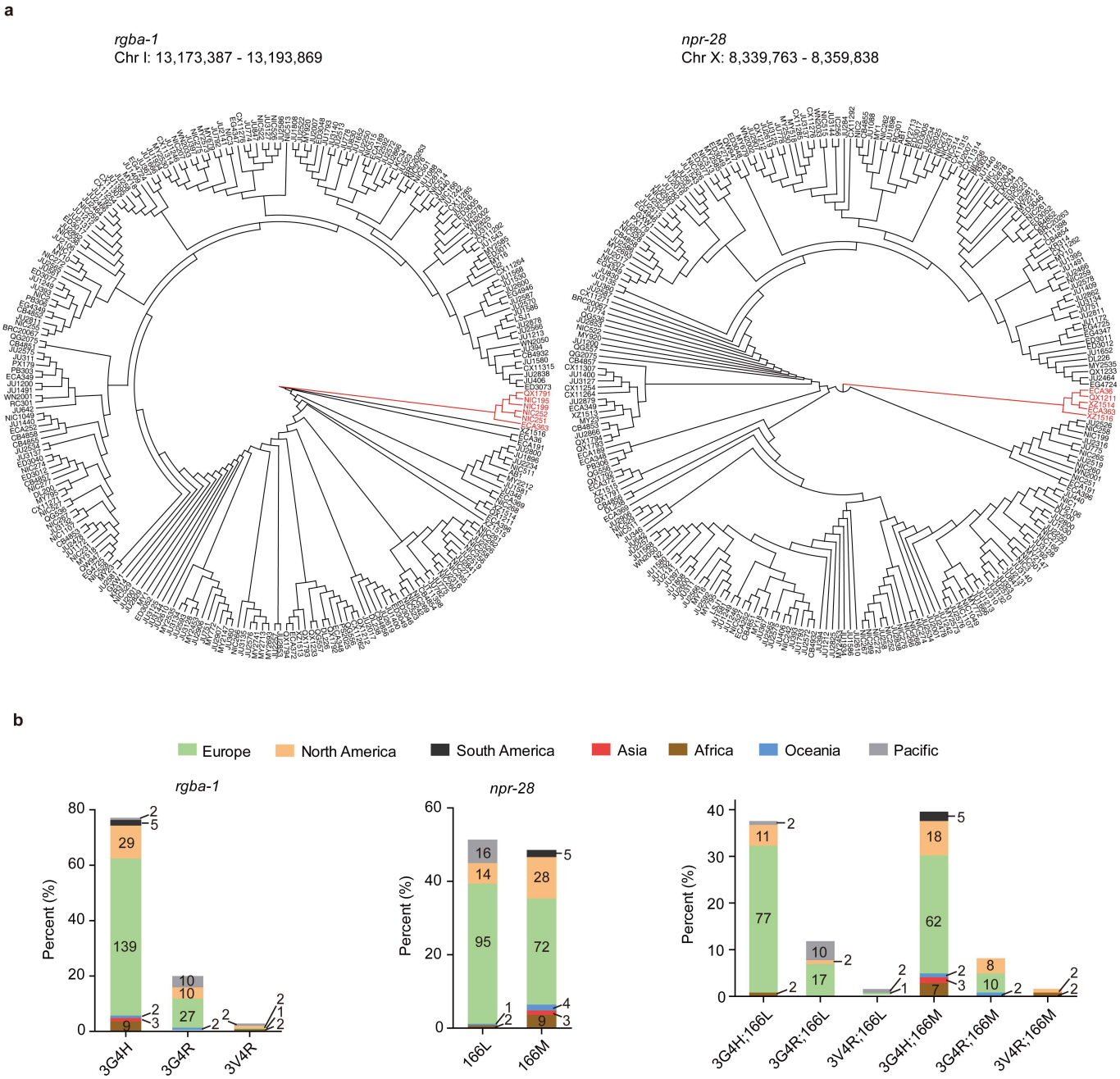

Extended Data Figure 9 | UPGMA trees across 249 natural isolates, and global distribution of *rgba-1* and *npr-28* alleles. a, UPGMA trees were generated using DNA polymorphisms within a 20-kb region surrounding *rgba-1* (left) or *npr-28* (right). The minimum basal branch and its descendants are marked in red, and the size of the minimum basal branch $n - \psi = 6$ and 5 for *rgba-1* and *npr-28*, respectively. **b**, Frequency and global distribution of *rgba-1* and *npr-28* alleles among wild strains. The number of wild strains is indicated inside or near the bar.

Extended Data Table 1 | Real-time PCR analysis of transcription of SIR-2.1 downstream genes

	Strain								
Gene	N2	*rgba-1(yfh081)*	*npr-28(yfh004)*	*rgba-1;npr-28*	*sir-2.1(ok434)*	*rgba-1;sir-2.1*	*npr-28;sir-2.1*	CB4856	AB3
hsp-6	1	1.21 ± 0.03**	1.40 ± 0.06**	1.25 ± 0.03*	0.74 ± 0.23	1.04 ± 0.04	1.01 ± 0.34	1.31 ± 0.04*	1.27 ± 0.07*
hsp-60	1	1.35 ± 0.07*	1.54 ± 0.15*	1.42 ± 0.10*	0.58 ± 0.21	1.05 ± 0.06	0.9 ± 0.09	1.44 ± 0.02**	1.70 ± 0.15**
clpp-1	1	1.22 ± 0.03**	1.39 ± 0.10*	1.27 ± 0.07*	0.62 ± 0.18	1.04 ± 0.12	0.8 ± 0.19	1.26 ± 0.04*	1.61 ± 0.13**
hsp-4	1	1.08 ± 0.10	1.09 ± 0.07	N.E.	N.E.	N.E.	N.E.	N.E.	N.E.
sod-1	1	1.02 ± 0.10	0.90 ± 0.08	N.E.	N.E.	N.E.	N.E.	N.E.	N.E.
sod-2	1	1.00 ± 0.04	1.10 ± 0.07	N.E.	N.E.	N.E.	N.E.	N.E.	N.E.
sod-3	1	1.00 ± 0.10	0.62 ± 0.10	N.E.	N.E.	N.E.	N.E.	N.E.	N.E.
sod-4	1	1.04 ± 0.08	1.06 ± 0.03	N.E.	N.E.	N.E.	N.E.	N.E.	N.E.
sod-5	1	1.31 ± 0.11	0.76 ± 0.09	N.E.	N.E.	N.E.	N.E.	N.E.	N.E.
ctl-1	1	0.99 ± 0.06	1.02 ± 0.08	N.E.	N.E.	N.E.	N.E.	N.E.	N.E.
ctl-2	1	1.07 ± 0.02	0.94 ± 0.13	N.E.	N.E.	N.E.	N.E.	N.E.	N.E.
pck-1	1	0.71 ± 0.35	0.83 ± 0.26	N.E.	N.E.	N.E.	N.E.	N.E.	N.E.
pck-2	1	0.96 ± 0.05	0.89 ± 0.03	N.E.	N.E.	N.E.	N.E.	N.E.	N.E.

Transcriptional expression levels of UPR^{mt}-related, catabolic enzyme, and ROS-scavenger enzyme genes in *C. elegans* males at day 5 of adulthood. All values were normalized to those of N2 worms. Data shown are mean ± s.e.m. *$P < 0.05$, **$P < 0.01$ (two-sided *t*-test). N.E., not examined.

nature research

Corresponding author(s): Shi-Qing Cai

☐ Initial submission ☐ Revised version ☒ Final submission

Life Sciences Reporting Summary

Nature Research wishes to improve the reproducibility of the work that we publish. This form is intended for publication with all accepted life science papers and provides structure for consistency and transparency in reporting. Every life science submission will use this form; some list items might not apply to an individual manuscript, but all fields must be completed for clarity.

For further information on the points included in this form, see Reporting Life Sciences Research. For further information on Nature Research policies, including our data availability policy, see Authors & Referees and the Editorial Policy Checklist.

Experimental design

1. Sample size

Describe how sample size was determined.

No statistical method was used to predetermine sample size. The sample sizes in our experiments were determined according to related analysis in literatures.

2. Data exclusions

Describe any data exclusions.

For lifespan assays, worms that crawled off the plate could cause irregular death and were not included in the data. For male mating assay, mating plates with males or hermaphrodites that crawled out the plate during the assay could not allow for standard mating condition and thus were not included in the analysis. Both exclusion criteria has been established previously.

3. Replication

Describe whether the experimental findings were reliably reproduced.

Experimental findings were reliably reproduced.

4. Randomization

Describe how samples/organisms/participants were allocated into experimental groups.

For lifespan assays and behaviour analysis, healthy late L4 or young adult worms were picked and raised on plates with bacteria lawn, and they were chosen unbiasedly for experiments to ensure randomization.

5. Blinding

Describe whether the investigators were blinded to group allocation during data collection and/or analysis.

For behavioural and lifespan experiments, the experimenters were blind to the genotype or dsRNA treatment. For immunocytochemical assays, the experimenter who performed data analysis was blind to the allele types.

Note: all studies involving animals and/or human research participants must disclose whether blinding and randomization were used.

6. Statistical parameters

For all figures and tables that use statistical methods, confirm that the following items are present in relevant figure legends (or in the Methods section if additional space is needed).

n/a	Confirmed
☐	☒ The exact sample size (*n*) for each experimental group/condition, given as a discrete number and unit of measurement (animals, litters, cultures, etc.)
☐	☒ A description of how samples were collected, noting whether measurements were taken from distinct samples or whether the same sample was measured repeatedly
☐	☒ A statement indicating how many times each experiment was replicated
☐	☒ The statistical test(s) used and whether they are one- or two-sided (note: only common tests should be described solely by name; more complex techniques should be described in the Methods section)
☐	☒ A description of any assumptions or corrections, such as an adjustment for multiple comparisons
☐	☒ The test results (e.g. *P* values) given as exact values whenever possible and with confidence intervals noted
☐	☒ A clear description of statistics including central tendency (e.g. median, mean) and variation (e.g. standard deviation, interquartile range)
☐	☒ Clearly defined error bars

See the web collection on statistics for biologists for further resources and guidance.

Software

Policy information about availability of computer code

7. Software

Describe the software used to analyze the data in this study.

For most analysis, GraphPad Prism7.0 software (GraphPad Software, Inc.) was used. For locomotion speed measurement, Image J with wrMTrck plug-in (National Institutes of Health) was used and data were fitted by GraphPad. For RGBA-1 derived peptides isolation and identification, Thermo Proteome Discoverer software (Thermo Fisher Scientific) was used, and for RGBA-1-2b quantification, Xcalibur 4.0 software (Thermo Fisher Scientific) was used. Fluorescence intensity was quantified using NIS-Elements AR 3.2 (Nikon). Phylogenetic trees were reconstructed using MEGA 7. Whole-genome sequence data of SQC0002 were analysed by CloudMap using "Hawaiian variant mapping with WGS data" workflow.

For manuscripts utilizing custom algorithms or software that are central to the paper but not yet described in the published literature, software must be made available to editors and reviewers upon request. We strongly encourage code deposition in a community repository (e.g. GitHub). *Nature Methods* guidance for providing algorithms and software for publication provides further information on this topic.

Materials and reagents

Policy information about availability of materials

8. Materials availability

Indicate whether there are restrictions on availability of unique materials or if these materials are only available for distribution by a for-profit company.

There are no restrictions on availability of materials.

9. Antibodies

Describe the antibodies used and how they were validated for use in the system under study (i.e. assay and species).

Anti-Calnexin antibody (Rabbit polyclonal to Calnexin), abcam, cat. #: ab22595, lot#: GR294502-1, citation:J Biol Chem 285, 35519-35527, doi:M110.162438 [pii]10.1074/jbc.M110.162438 (2010), and the antibody was validated (i.e assay and species) by the company using Calnexin knock out cell lines, please refer to the manufacturer's description: www.abcam.com/calnexin-antibody-ab22595.html. Alexa-Fluor-488-conjugated Donkey anti-Rabbit IgG (H+L) Secondary Antibody, Invitrogen, cat. #: A-21206, lot #: 1754421, citation: Assay Drug Dev Technol 8, 186-199, doi:10.1089/adt.2009.0213 (2010), and manufacture's description: https://www.fishersci.com/shop/products/alexa-fluor-488-donkey/a21206. Anti-mCherry antibody (Mouse Monoclonal), Earthox, cat. #: E022110-01, lot. #:MY2301, citation: Cell Death and Disease (2016) 7, e2068; doi:10.1038/cddis.2015.300, and the antibody was optimized and validated (i.e assay and species) by the company, please refer to the manufacture's description: www.earthox.net/anti-mcherry-tag-mouse-monoclonal-antibody. We also have validated this antibody using cell lines expressing mCherry fused proteins with empty vectors as a negative control.

10. Eukaryotic cell lines

a. State the source of each eukaryotic cell line used.

COS-7 (cat. #: SCSP-508) and HEK293T (cat. #: SCSP-502) cell lines were obtained from cell bank of Chinese Academy of Sciences.

b. Describe the method of cell line authentication used.

These cell lines have been validated using the short tandem repeat (STR) profiling method by the cell bank of Chinese Academy of Sciences.

c. Report whether the cell lines were tested for mycoplasma contamination.

No

d. If any of the cell lines used are listed in the database of commonly misidentified cell lines maintained by ICLAC, provide a scientific rationale for their use.

No commonly misidentified cell lines were used.

Animals and human research participants

Policy information about studies involving animals; when reporting animal research, follow the ARRIVE guidelines

11. Description of research animals

Provide details on animals and/or animal-derived materials used in the study.

The study used wild isolates and mutants of Caenorhabditis elegans. Wild isolates, EG6699, SJ4100, sir-2.1(ok434), hsf-1(sy441) and unc-54(e190) worms were obtained from the Caenorhabditis Genetics Center. Other worm strains were generated in our lab. Males at day 1 - day 7 of adulthood were used for male mating behaviours. Hermaphrodites at day 1 - day 14 of adulthood were used for pharyngeal pumping and locomotion assays. Hermaphrodites were used for lifespan assay. Pbas-1::bas-1::gfp transgenic hermaphrodites at day 1 or day 9 of adulthood were used to determine BAS-1::GFP fluorescence intensity. Worms at day 1 of adulthood were used for peptide isolation and rgba-1, npr-28 expression pattern examination. Young adult hermaphrodites in hsf-1(sy441) background were used for RGBA-1 secretion assay. Phsp-6::gfp transgenic hermaphrodites at day 1 of adulthood were used for measuring UPRmt marker Phsp-6::GFP fluorescence intensity. Males at day 5 of adulthood were used to perform RT-PCR analysis of transcription of SIR-2.1 downstream genes.

Policy information about studies involving human research participants

12. Description of human research participants

Describe the covariate-relevant population characteristics of the human research participants.

The study did not involve human research participants.